Radial Parallel Plate Flow with Mechanical Agitation

by

Jackson T. Crane

Submitted to the Department of Mechanical Engineering
in partial fulfillment of the requirements for the degree of

Bachelor of Science in Mechanical Engineering

at the

MASSACHUSETTS INSTITUTE OF TECHNOLOGY

June 2013

Author .....
Department of Mechanical Engineering
May 10, 2013

Certified by .....
J.G. Brisson
Professor of Mechanical Engineering
Thesis Supervisor

Accepted by .....
Annette Hosoi
Professor of Mechanical Engineering
Undergraduate Officer

Radial Parallel Plate Flow with Mechanical Agitation

by

Jackson T. Crane

Submitted to the Department of Mechanical Engineering
on May 10, 2013, in partial fulfillment of the
requirements for the degree of
Bachelor of Science in Mechanical Engineering

Abstract

Computer processors have significant and rising cooling requirements, with electronics cooling estimated to consume 1% of global energy consumption. An integrated fan heat sink was designed to help alleviate this issue, and is designed to simultaneously improve heat transfer and efficiency. Current designs chiefly focus on improving heat transfer without concern for overall energy efficiency. The novel heat sink integrates fans directly into a heat pipe loop, with impellers located in between series of parallel condensers, with a single evaporator located on the interface of the heated chip. The proximity of the fans to the hot surfaces improves overall heat transfer while maintaining a high efficiency.

The impellers push air radially outward through parallel heated plates, with an air intake from the center. Little research has been done on the fluid mechanic properties of this physical situation, particularly with an impeller agitating the air stream. For the design of the integrated heat sink, it is desirable to understand the thermal properties of the channel in terms of various parameters such as impeller geometry and speed, gap thickness, and mass flow rates. Experiments were performed to determine the local heat transfer coefficient between two heated plates with the presence of an impeller with different parameters. The results from these tests were used to infer the properties of the flow. These experiments are designed to replicate the flow in one distinct channel in the integrated fan heat sink, and can be expanded to observe the convective heat transfer characteristics of the entire device.

It was found that the impellers enhance heat transfer significantly beyond that of inducing flow, by up to five times. It was then shown that the presence of impeller blades have a direct effect on the heat transfer by comparing different size impellers. Both mass flow rate (radial Reynolds number) and rotational velocity of the impeller were found to have significant, independent, effects on heat transfer. The cause of the increase in heat transfer from the blades is from an increase in turbulent mixing.

Thesis Supervisor: J.G. Brisson
Title: Professor of Mechanical Engineering

Acknowledgments

I would first like to acknowledge Professor Brisson for teaching and challenging me about thermal fluids engineering, research, and writing. I have valued our meetings tremendously and grown as a researcher and student from his mentorship. Wayne Staats has also provided invaluable assistance throughout the research. He left me not only with his experimental apparatus which I used for the duration of my thesis, but consistently provided his instruction, insight, and ideas.

There were a few graduate students who were kind enough to help me in my research. I would like to thank: Kevin Cedrone for lending a mass flow meter; Andrej Lenert for explaining the thermal camera; Daniel Hanks for ordering me a new cooling fan; and Nicholas Roche for teaching me about the PHUMP.

My family and friends deserve mention as well, particularly my mother and father for their constant love and support, my brother for his intellectual vibrancy, and my late grandfather for inspiring greatness in all aspects of life.

Contents

List of Figures

List of Tables

Chapter 1

Introduction

1.1 Motivation

Electronics cooling comprises an estimated 1% of overall electricity consumption worldwide. This can be expected to increase as electronics become more universal and powerful [7]. As processor chips are performing a greater number of operations per unit volume, their power consumption also correspondingly increases. This, in conjunction with the global energy issues, necessitates advances in thermal management.

To tackle this issue, an integrated fan heat sink was created by Allison et al [3], and is shown in Figure 1-1. This heat sink is a multi-layer device with impellers between condenser plates. An evaporator is located at the bottom of the device to complete a heat pipe loop, which capitalizes on the high enthalpy of evaporation of fluids. It is believed that this configuration can lead to significantly more efficient heat sinks than the traditional finned designs.

To create an efficient integrated fan heat sink, effective heat transfer from the condenser plates is required. To achieve this, impellers are used to induce forced convection. Because of the unique physical situation, little research has been done to characterize the fluid mechanic properties of outward radial fluid flow between two plates with an impeller situated in between the plates. It is specifically important to characterize the heat transfer coefficient

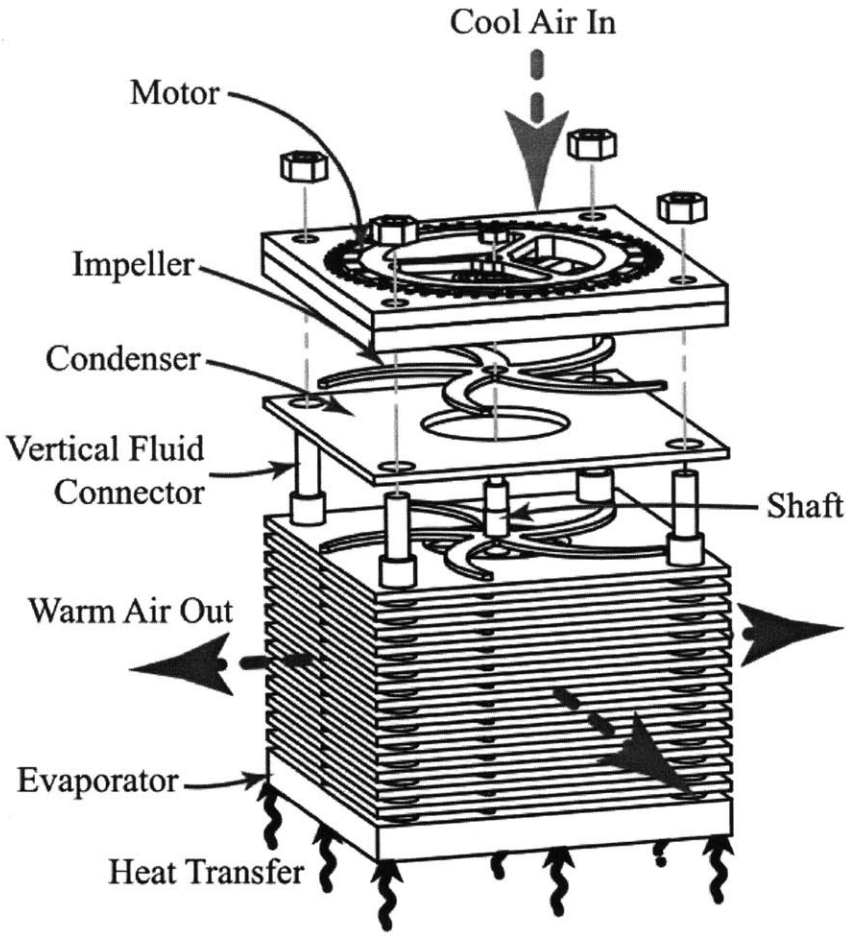

Figure 1-1: A schematic of the multi-layer integrated fan heat sink. Image taken from Allison et al [3].

as a function of different parameters such as impeller speed, distance between the impeller and the stator plate, boundary conditions, and impeller geometry.

Mochizuki and Yang [4] have done considerable research about the fluid mechanic properties of outward radial flow between two parallel disks. They have also researched the average and local heat transfer coefficients of such flow in [5]. While useful for experimental comparison, this research does not include impellers, but rather uninterrupted radial flow. Staats [6] did considerable research about the pumping properties and average heat transfer coefficients of various impellers. He also did some local heat transfer coefficient tests for

a limited set of impellers and other parameters. The purpose of the present research is to continue to examine the local heat transfer coefficient induced by various parameters and use these studies to elucidate the fluid mechanic phenomena occurring between the parallel plates. With this information it is possible to make more informed decisions about the design of the integrated fan heat sink. It also serves to advance the knowledge of fluid mechanic properties in channels with continuous agitation.

1.2 Reynolds Number in Radial Parallel Disc Flow

When characterizing flow, a particular dimensionless number, Reynolds number (Re), is useful. The Reynolds number represents the ratio of inertial forces to viscous forces, defined as

$$Re = \frac{\rho v D_h}{\mu} \tag{1.1}$$

where ρ is the fluid density, v is the bulk velocity, D_h is the hydraulic diameter, and μ is the kinematic viscosity. Hydraulic diameter is defined as

$$D_h = \frac{4A}{P} \tag{1.2}$$

where A is the cross-sectional flow channel area, and P is the flow perimeter [8]. The radial parallel disc flow geometry with an impeller is shown in Figure 1-2. Applied here, hydraulic diameter is calculated as:

$$D_h = \frac{4 b_{gap} 2\pi r}{4\pi r} = 2 b_{gap} \tag{1.3}$$

So, in the present physical configuration, the Reynolds number becomes:

$$Re_{D_h} = \frac{2\rho v b_{gap}}{\mu} \tag{1.4}$$

Calculating the bulk fluid velocity with the presence of an impeller, v, is more complex.

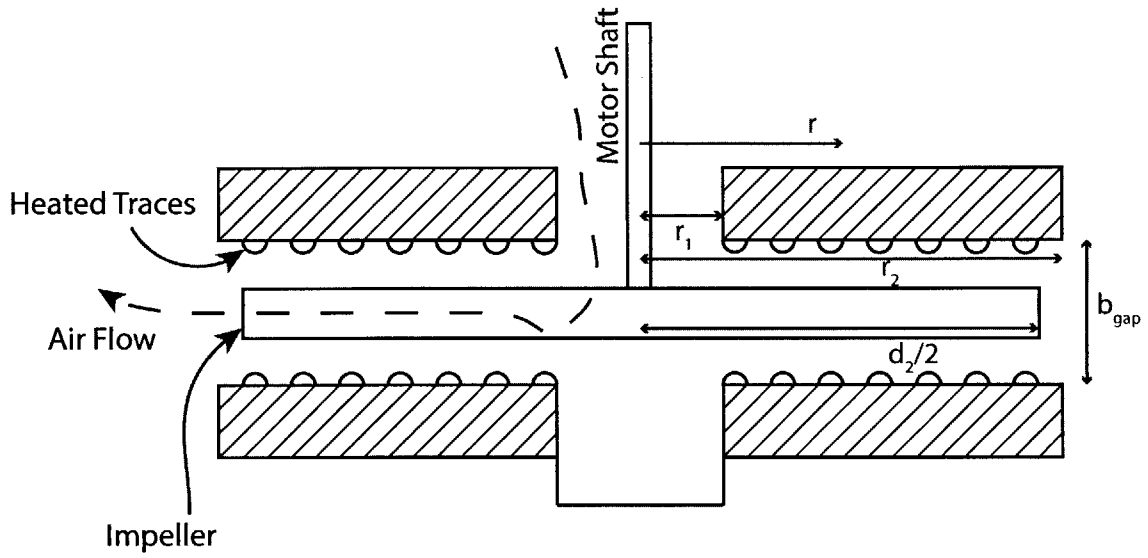

Figure 1-2: A schematic of the flow channel that is used in this work. Not to scale.

In pure radial flow, given the mass flow rate (measured in the experimental apparatus), it is simple to calculate the velocity.

$$v_{radial} = \frac{\dot{m}}{2\pi r b_{gap}} \tag{1.5}$$

Using the radial velocity yields a radial Reynolds number, which will be used extensively in analysis.

$$Re_{radial} = \frac{\dot{m}}{\mu\pi r} \tag{1.6}$$

The fluid velocity is expected to be significantly higher than what the mass flow rate suggests because the impeller moves the fluid azimuthally as it spins. Initially it was attempted to predict the effective velocity based on the addition of vectors of the radial velocity and rotational velocity, as depicted by Figure 1-3. For a first order estimate it was predicted that the rotational velocity of the fluid is equal to the velocity of the impeller. With this estimated fluid velocity, the rotational velocity component dominates the radial velocity component.

This does not adequately predict the physics of the situation because an increase in mass flow, linked to the radial velocity, increases the capacity flow rate of the fluid, whereas the azimuthal velocity component does not. Staats [6] found that these two effects were independent, and his correlations are comprised of the addition of radial Reynolds number and rotational Reynolds number. Rotational Reynolds number is defined as:

$$Re_\omega = \frac{\rho \omega d_2^2}{4\mu} \tag{1.7}$$

In radial parallel disc flow, three separate flow regimes have been observed: laminar flow, laminar oscillating flow, and turbulent flow [4]. Laminar flow is characterized by straight, ordered flow with limited to no mixing. Mochizuki observed laminar flow in parallel radial disc flow at radial Reynolds numbers below 1200.

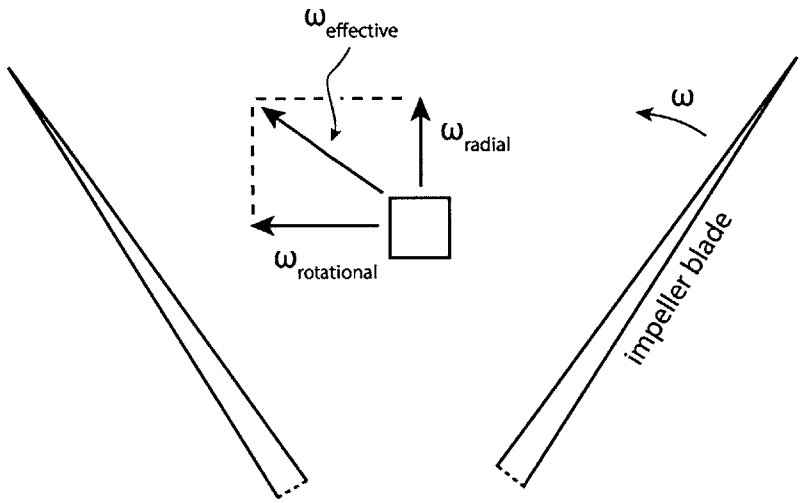

Figure 1-3: A representation of a differential element of fluid from which the effective Reynolds number is derived.

Laminar oscillating flow occurs when there is separation of the shear-layer from the discs. This is caused by the creation of vortices, which then decay away, causing an oscillating laminar flow. This was observed with radial Reynolds numbers between 1200 and 5000. Turbulent flow occurs at Reynolds numbers above 5000, and is associated with constant

mixing and chaotic flow characteristics.

1.3 Heat Transfer Coefficient

The heat transfer coefficient, h is a measure of how effectively heat is convectively transferred from a surface to a fluid. In this work it is defined as:

$$h = \frac{Q}{A\Delta T} \tag{1.8}$$

where ΔT is defined as either:

$$\Delta T = T_{wall} - T_{air} \tag{1.9}$$

or:

$$\Delta T_{ITD} = T_{wall} - T_{inlet} \tag{1.10}$$

where ITD stands for the inlet temperature difference. When Equation 1.10 is used, the heat transfer coefficient calculated is referred to as h_{ITD}, while when the more traditional Equation 1.9 is used, the heat transfer coefficient is simply h. Using the two different definitions becomes useful when examining the end of the channel because of significant recirculatory effects that are not accounted for in analysis. It should be approached with care, however, because these two heat transfer coefficients are not directly comparable.

To nondimensionlize heat transfer coefficient, Nusselt number is used. Nusselt number is the ratio of convective heat transfer to conductive heat transfer. Two different Nusselt numbers are defined, one in terms of the hydraulic diameter, and one in terms of the flow length.

$$Nu_{D_h} = \frac{Convective\,Heat\,Transfer}{Conductive\,Heat\,Transfer} = \frac{hD_h}{k} \tag{1.11}$$

where D_h is the hydraulic diameter; in this experiment it is two times the gap, $2b_{gap}$.

$$Nu_L = \frac{hL}{k} \tag{1.12}$$

L is the flow length, or $r_2 - r_1$. Nu_{D_h} is useful when comparing our experimental results to other previous work, while Nu_L is useful when comparing different results within our data set. Although Nu_L is not the traditional definition, it is useful because it is found that there is little relation between gap thickness and heat transfer, so using hydraulic diameter to compare between trials with different gap thicknesses will report effects that are not present. Typically a Nusselt number between 1 and 10 is indicative of laminar flow, and larger Nusselt numbers, between 100 and 1000 are observed in turbulent flow [1].

1.4 Thermal Boundary Layers

Boundary layers are created along a surface over which flow travels. A fluid at the interface of a solid will have zero velocity, and then slow the adjacent fluid particles. This causes a region close to the bounding surface to have a significantly slower velocity than the bulk of the fluid. The boundary layer is typically defined as the region up to which 99% of the free stream velocity is reached. This boundary layer, associated with the velocity of the stream is correspondingly called the velocity boundary layer.

Similar to the velocity layer, a thermal boundary layer forms over a surface if there is a temperature difference between the bounding surface and the fluid stream. The fluid particles very close to the surface reach thermal equilibrium with that surface, and transfer heat with the particles around it. This causes a thermal gradient to form, and the region where this thermal gradient is active is known as the thermal boundary layer. Analagous to the velocity boundary layer, the thermal boundary layer is the region up to which $[(T_s - T)/(T_s - T_\infty)]$ $= 0.99$ [1].

Close to the bounding surface the fluid velocity is near zero, and so the primary mode of heat transfer is through conduction. The thermal conductivity of air is extremely low, so this creates a high thermal resistance. The thickness of the thermal boundary layer then has

a strong influence on the overall heat transfer characteristics of a system.

The flow regime has an important effect on the characteristics of the boundary layer. In laminar flow, the velocity boundary layer continually increases in thickness along the length of a bounding surface. This causes the thermal boundary layer to increase in thickness as well, thus impeding heat transfer further down a plate. When examining the local heat transfer coefficient along a flat plate, it will be observed that the heat transfer is high at in the inlet of the plate because of the nonexistent boundary layer, and then decays rapidly as the boundary layer is formed.

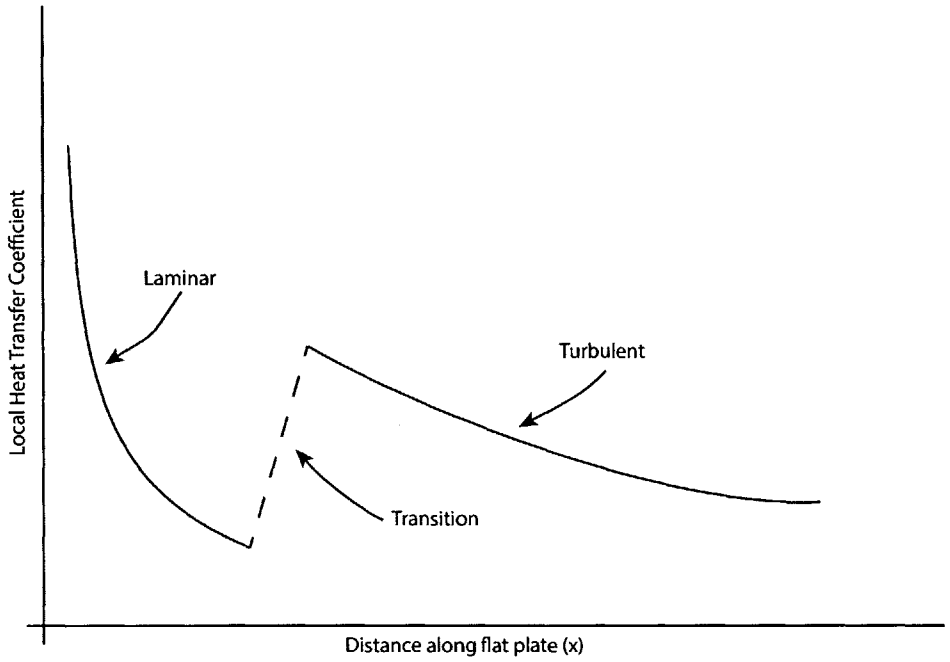

Figure 1-4: A representation of local heat transfer coefficient as a function of distance along a plate kept at constant temperature. Adapted from Incropera [1].

The turbulent boundary layer is more complex. Near the bounding surface, the flow is ordered, and the velocity profile is approximately linear. This is called the viscous sublayer. Further from the surface the mixing effects from turbulent flow become increasingly dominant. The region in which viscous effects and turbulent mixing are comparable is called the buffer layer, which then becomes the turbulent zone in the bulk of the stream. These

effects are present both in velocity and thermal turbulent boundary layers. The nonlinearity in turbulent flow causes mixing in the turbulent zone and to a lesser degree in the buffer zone. This mixing enhances heat transfer significantly because the length in which heat transfer is dominated by conduction is decreased. It can be observed that in a flow stream that transitions from laminar to turbulent flow, the local heat transfer coefficient increases significantly in the turbulent zone, as shown in Figure 1-4.

1.5 Surface Renewal

One hypothesis which describes the heat transfer enhancement due to a rotating impeller is 'surface renewal,' described by Hagge et al [2]. In this process as a blade passes over a region of the plate, part of the boundary layer on that plate is wiped away. This thinner boundary layer causes a higher heat transfer rate than that of the previously thicker layer. In this model, higher rotational velocity and blade count equally enhance heat transfer, because the surface renewal frequency, f, dictates the heat transfer. Hagge shows that the heat transfer coefficient due to surface renewal is:

$$h = 2\sqrt{\frac{k\rho c_p}{\pi}}\sqrt{f}. \tag{1.13}$$

It is unclear whether this theory applies in the radial parallel plate geometry, because the research on surface renewal has before been in significantly different physical situations. Figure 1-5 shows the expected relationship between boundary layer thickness and heat transfer coefficient as a function of time. The rises in heat transfer coefficient are caused by a dip in the boundary layer thickness, which is caused by a blade wipe. The boundary layer thickness is expected to rise with the square root of time, with the heat transfer proportional to the inverse of thickness.

A Reynolds number based on frequency renewal is conceived, similar to a rotational Reynolds number. It is calculated as:

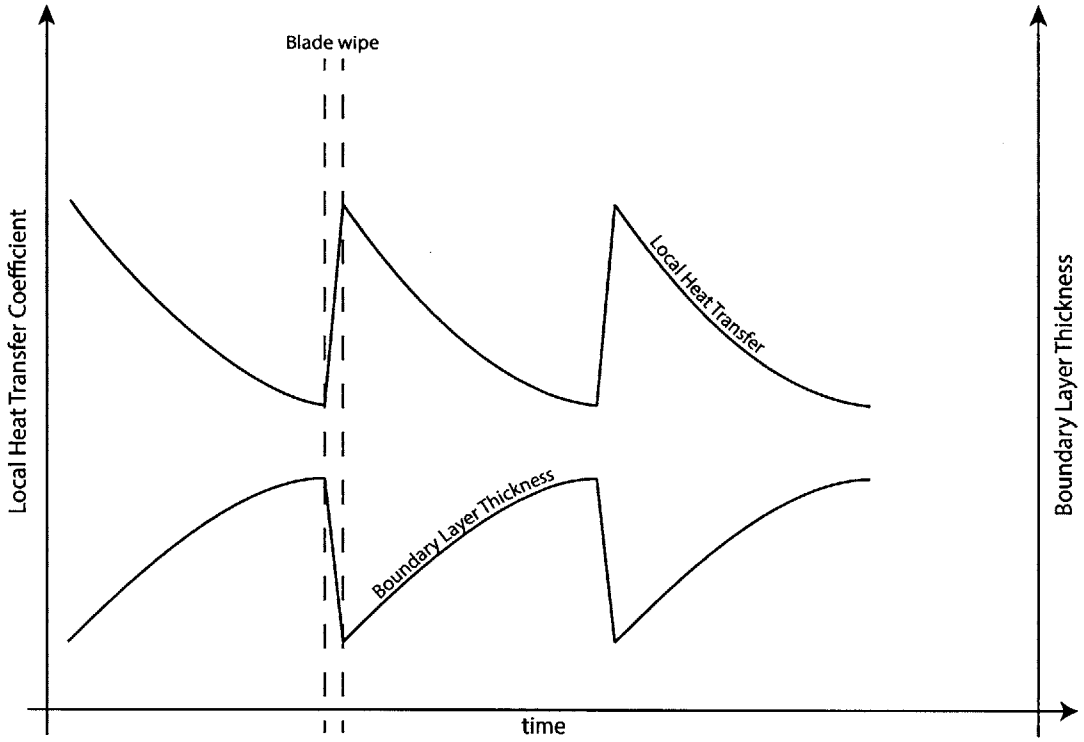

Figure 1-5: A heuristic representation of local heat transfer coefficient and boundary layer thickness as a function of time, with two blade wipes shown.

$$Re_f = \frac{\rho \omega n_b d_2^2}{4\mu} \tag{1.14}$$

where n_b is the number of blades on a particular fan and d_2 is the outer diameter of the fan.

Chapter 2

Experimental Procedure

A host of experiments characterizing the local heat transfer coefficient of parallel disks with an impeller were performed. The experimental setup used is described in Staats' work [6]. A few minor adjustments were made to optimize the process of recording local heat transfer reliably and repeatedly. The experimental setup, as shown in Staats' work, is copied in Figure 2-2.

The apparatus under normal operation has an inlet at the top, with an attached air filter. The air then flows through a mass flow meter. Directly downstream from the flow meter is a butterfly valve throttle, which is used to control the mass flow during fan experiments. The air then flows through an air plenum with a baffle, followed by a screen. This minimizes jetting from the throttle and smooths variation in flow. A cross section of the air plenum is shown in Figure 2-1. The air then exits through the fan inlet, where it passes between the parallel heated stator plates, and is finally discharged to the ambient. In between these plates sits an impeller, actuated by a motor contained in the air plenum. The bottom of the apparatus, with the stator plates and impeller, is shown schematically in Figure 1-2.

The heated stator plates have a series of twelve heated traces, allowing for independent heated zones. With the combination of a closed feedback loop, this allows the stator plates to be operated at both constant temperature and constant heat flux boundary conditions. Thermocouples are attached to each trace on the top and bottom stator plate. In addition

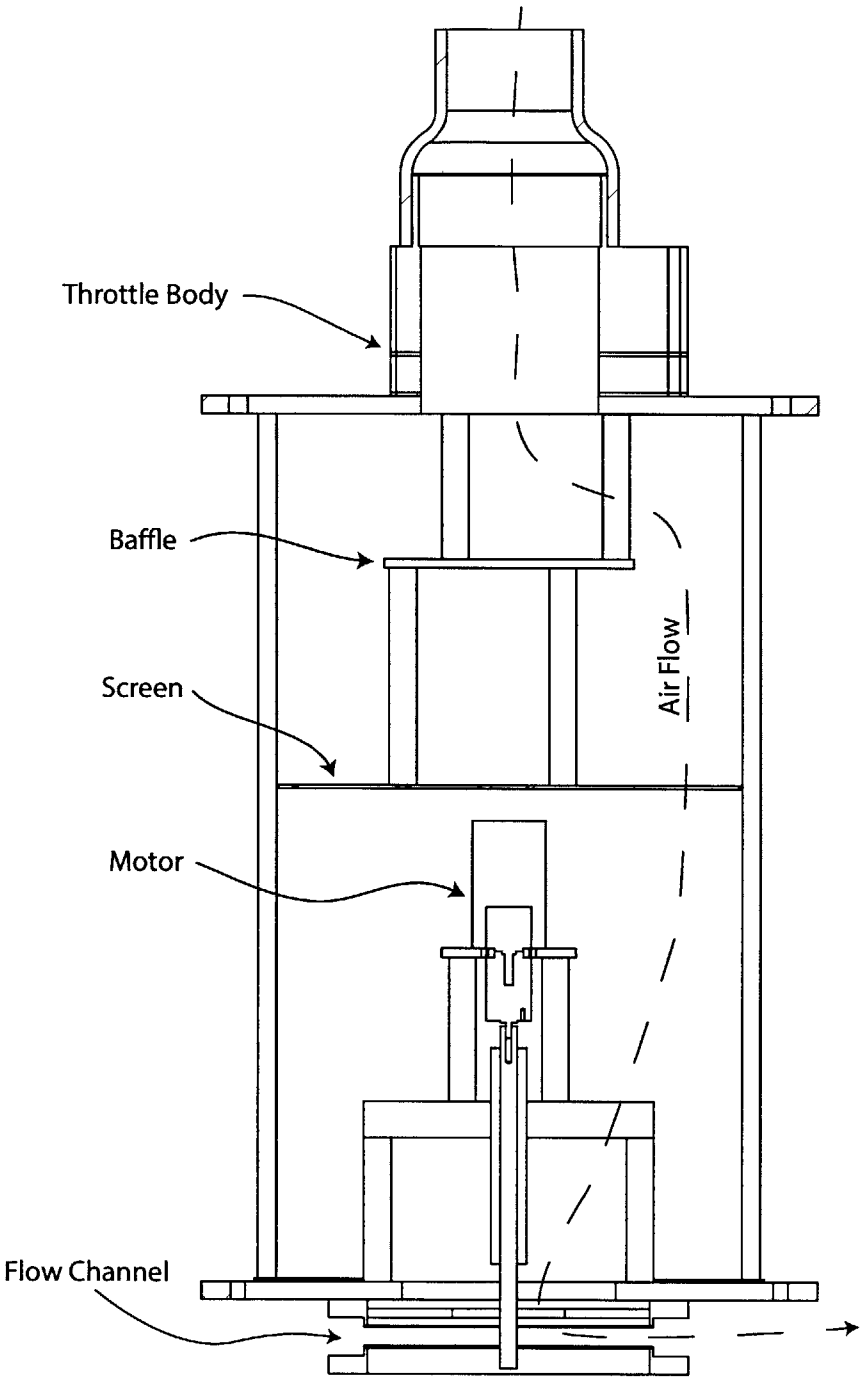

Figure 2-1: A cross section of the air plenum, with relevant structures labeled.

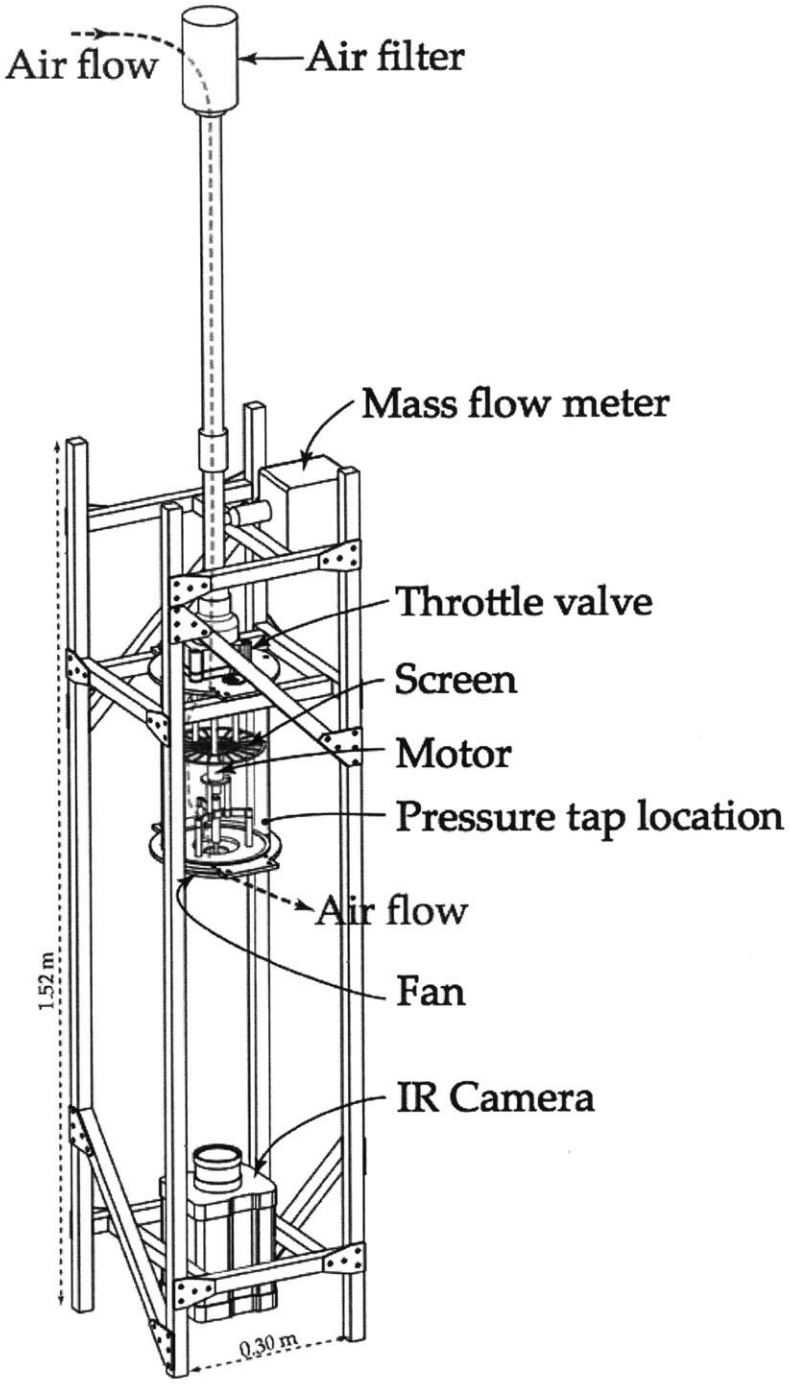

Figure 2-2: Diagram of experimental setup, originally from Staats' work [6]. This shows the air flow, which travels from the air filter, down through the mass flow meter, through the throttle, into the plenum, and finally out through the parallel disks.

to this, an IR camera is focused on the underside of the bottom stator plate. The IR camera allows for continuous temperature measurement along the bottom of the apparatus, which then yields continuous local heat transfer measurement. For more detailed information of the experimental setup and calibration, see Staats' work [6].

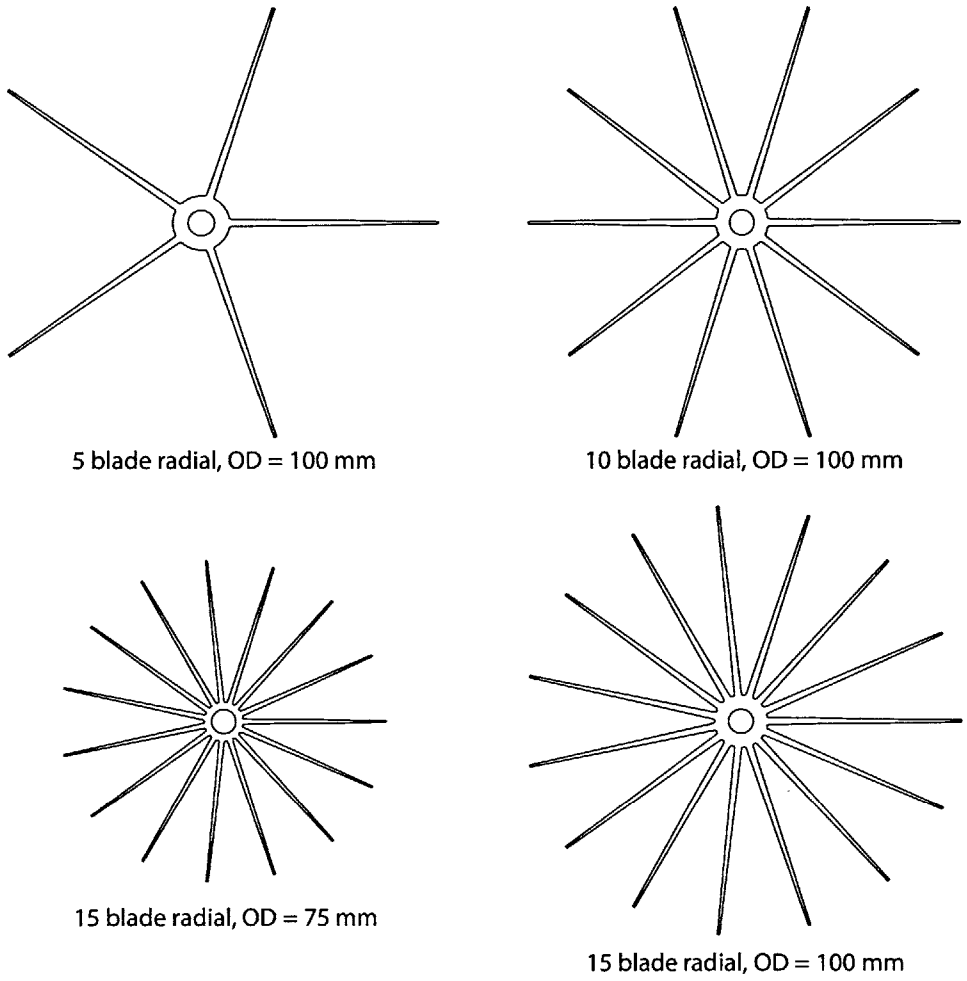

Figure 2-3: The four fans that are studied throughout the experiments.

Four different impellers were studied, and are shown in Figure 2-3. They all have identical geometry, with blades configured radially outward, but have different blade counts. It was desired to use simple, similar impellers to examine the fluid mechanic properties in the channel. For more thorough fan optimization, see Staats' work [6]. It is found there that

an impeller with curvature performs better than those with straight radial configurations. Five, ten, and fifteen blade fans were studied, all of which with an outer diameter of 100 mm, except a second fifteen blade fan, with an outer diameter of 75 mm. All fans are 1.5 mm thick.

Experiment	Blade Count	Fan OD (mm)	Gap (mm)	Boundary Condition
1	15	75	2.5	Const. Temp.
2	15	75	3.5	Const. Temp.
3	15	75	5	Const. Temp.
4	15	75	6.5	Const. Temp.
5	15	100	3.5	Const. Temp.
6	15	100	3.5	Const. Heat Flux
7	15	100	5	Const. Temp.
8	10	100	3.5	Const. Temp.
9	5	100	3.5	Const. Temp.

Table 2.1: Experimental matrix for experiments with impeller

2.1 Nitrogen Pressure Driven Flow

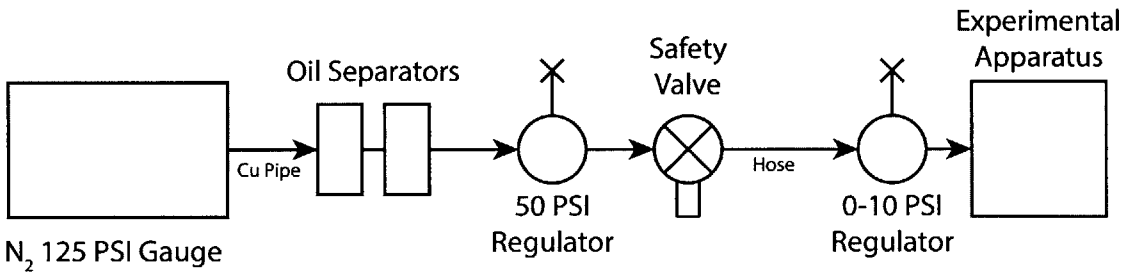

Figure 2-4: Schematic of the pressure driven nitrogen flow.

To provide a basis for comparison and to verify the experimental apparatus, a modification was made to induce pressure driven flow in the apparatus. The air filter shown in Figure 2-2 is replaced by a low pressure regulator (ControlAir Type 300 0-10 PSIG) which feeds nitrogen through the mass flow meter, and eventually down to the stator plates, as

described above. The setup is shown schematically in Figure 2-4, and a picture of the top of the apparatus in Figure 2-5. Manual manipulation of the regulator allows for control of the mass flow rate. Because of this, it is possible to replicate the range of mass flows that the impeller fan induces in the normal local heat transfer measurements.

The pressure regulator, in combination with an upstream high pressure regulator, causes difficulty in precisely controlling steady state mass flow rate. In future experimentation it would be preferable to use an electronically controlled pressure regulator with a closed feedback loop with the mass flow meter to allow for accurate control of mass flow rate. This would eliminate flow transients precluding the system from reaching a steady state.

Experiment	Gap (mm)	Boundary Condition	With Impeller
1	3.5	Const. Temp.	No
2	3.5	Const. Heat Flux	No
3	3.5	Const. Heat Flux	Yes
4	2	Const. Temp.	No
5	2	Const. Heat Flux	No
6	0.8	Const. Heat Flux	No

Table 2.2: Experimental matrix for experiments with nitrogen driven flow

During these experiments it was possible to induce flow between variable stator plate gap thicknesses, both with and without a stationary impeller. The results with an empty gap (no impeller installed) serve to validate the experimental apparatus and technique. Those with a stationary impeller inform whether the presence of the impeller itself changes the heat transfer characteristics of the channel.

2.2 Image Processing

A small modification to Staats' work in image processing was made. In place of recording a single image at each operating point, nine images were recorded at 5 Hz. These images were then averaged to create an image with less transients. This is aimed to reduce uncertainty in the thermal camera processing. Figure 2-6 shows the comparison of an averaged and a non averaged thermal image in a constant heat flux test. Although it is not immediately

evident, upon close inspection it can be observed that there is a decrease in transients from the thermal camera.

2.3 Mass Flow Control

It was desired to impose a constant mass flow rate for various experimental parameters. A control loop was designed to actuate the throttle using the mass flow meter as a sensor, until the desired mass flow rate was attained. A proportional integral controller was used with variable gains depending on the experimental parameters. Both the proportional and integral terms are scaled linearly with the rotational velocity of the impeller and the desired mass flow rate. The controller equation in the Laplace domain is:

$$C(s) = \frac{\alpha\beta}{\omega\dot{m}}\left(K_p + \frac{K_i}{s}\right) \tag{2.1}$$

The controller yields results with $\pm 10\%$ error, which was deemed acceptable for observing trends over large sets of data. It is believed that the controller could be improved to yield smaller steady state error.

Experiment	Blade Count	Fan OD (mm)	Gap (mm)	Boundary Condition
1	15	100	3.5	Const. Temp.
2	10	100	3.5	Const. Temp.

Table 2.3: Experimental matrix for experiments with constant mass flow rate

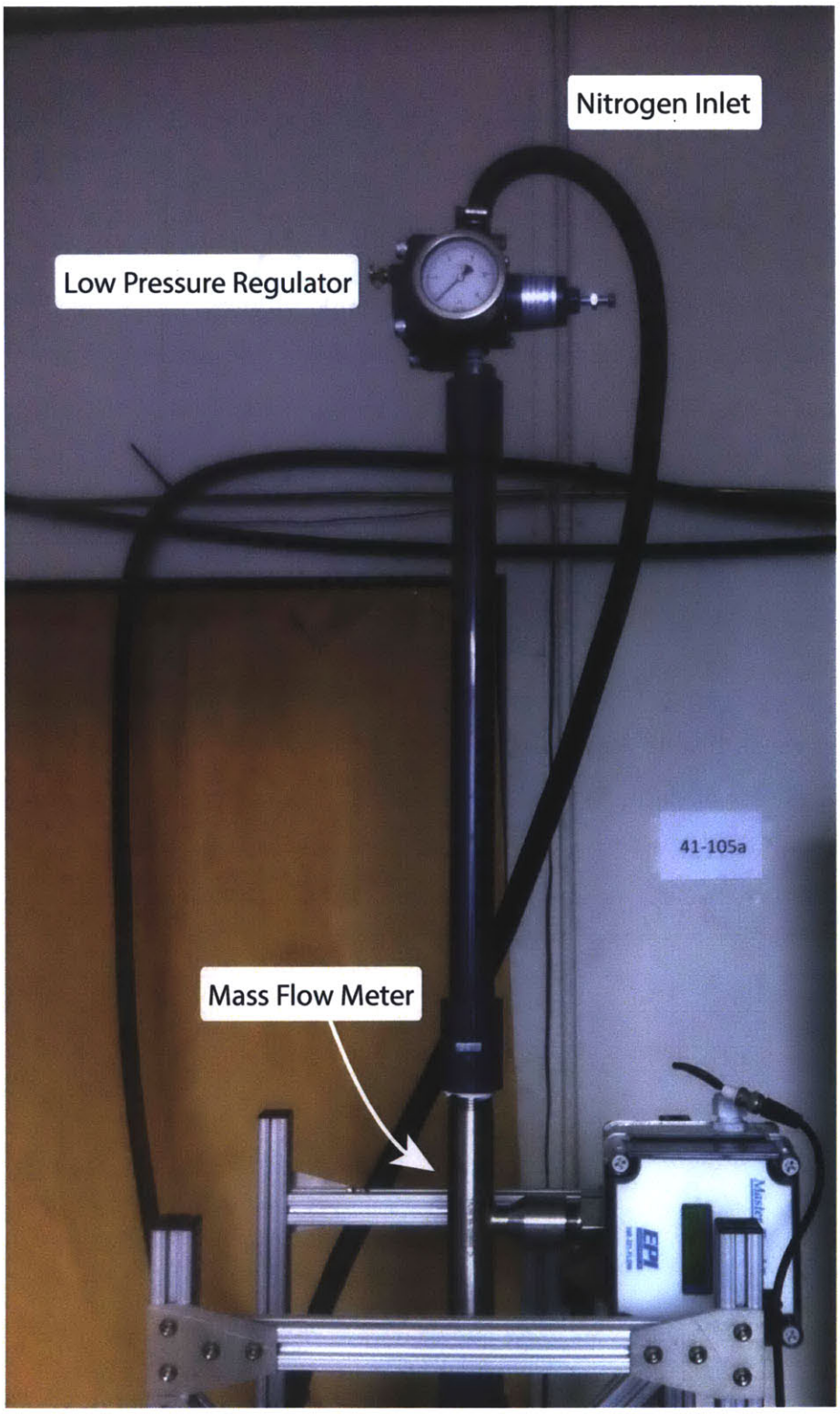

Figure 2-5: An image of the pressure driven flow modification.

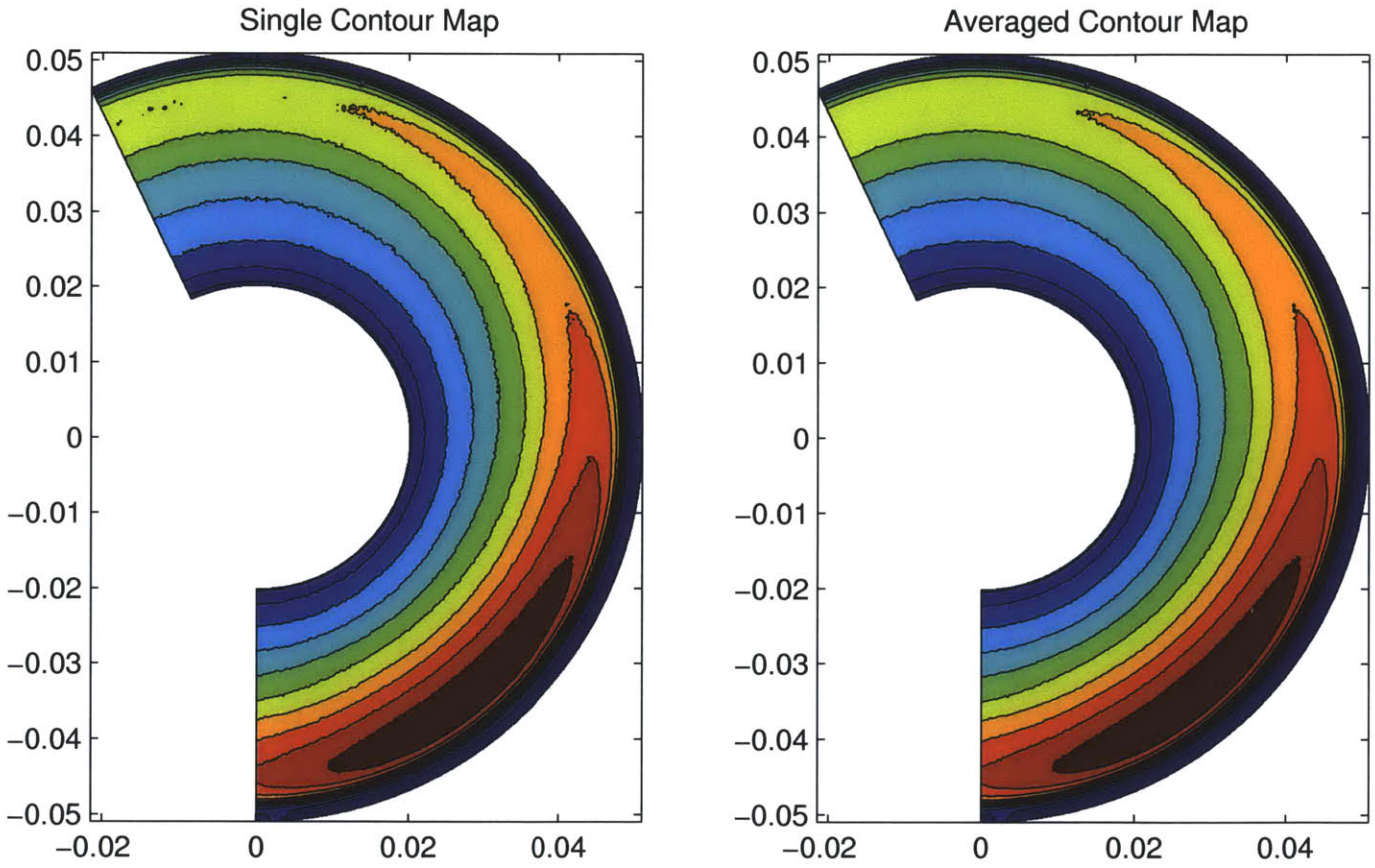

Figure 2-6: Comparison of thermal camera contour plots. The left image is a representative non-averaged image, and the image on the right is the same test averaged with eight other images. The transients are reduced in the right image.

Chapter 3

Experimental Results

The goal of the present research was to determine the mechanics of the heat transfer enhancement from the impeller. It is known that these impellers are capable of increasing the average heat transfer coefficient in a given channel [6], and there has been considerable optimization with the geometry of the impeller. It was postulated by Staats that the increase in heat transfer coefficient was because of the increase in turbulence in the channel. Vortices and flow instabilities are capable of increasing heat transfer and decreasing the boundary layer thickness, as discussed in Section 1.4. To investigate this, tests were performed with comparable Reynolds numbers, both with and without a spinning impeller.

Another hypothesis for the enhancement of heat transfer is due to a boundary layer shedding effect as the blades wipe across the plate. The boundary layer provides a high thermal resistance because it's low effective velocity implies a conductive rather than convective primary heat transfer mode. A thick boundary layer will then significantly impede heat transfer. If the blades of the impeller disturb the boundary layer with every pass, then it naturally follows that the heat transfer would be increased. An investigation comparing radial fans with differing blade counts was performed to examine the boundary layer shedding hypothesis.

First, however, experiments that could be compared directly to past work were performed to determine the validity of the experimental apparatus.

3.1 Pressure Driven Flow

To validate the experiments, pressure driven flow was examined without the presence of a fan. This was achieved by feeding nitrogen through the experimental apparatus (as shown in Section 2.1). A pressure regulator located at the top of the apparatus was manipulated, thereby allowing a controllable mass flow rate through the system. This allows the indirect control of mean radial Reynolds number for verification, and later for comparison to fan tests.

$$Re_{radial,mean} = \frac{\dot{m}}{\mu \pi r_{mean}} \tag{3.1}$$

where:

$$r_{mean} = \frac{r_2 - r_1}{2} \tag{3.2}$$

where r_2 is the radius of the exit of the channel, and r_1 is the radius of the inlet of the channel.

The experimental results were compared to Mochizuki and Yang [5] who characterized local Nusselt number on pressure driven flow between horizontal parallel disks. Nusselt number in terms of hydraulic diameter is defined in Equation 1.11 ($Nu = hD_h/k$). This is the same definition as that of Mochizuki and Yang.

T_{wall} is measured directly from the thermal camera, and T_{air} is found from a first law energy balance with the air. The first law energy balance does not account for air that is recirculated from the outlet of the channel. This air will carry away a significant amount of heat, which then leads to a high reported heat transfer coefficient. This is not from the heat transfer of the air recorded by the mass flow meter, and is therefore not properly accounted for in calculation. For much of the analysis, these erroneous regions are ignored.

The comparison between Mochizuki and Yang's local heat transfer results and our experimental verification is shown in Figure 3-1. The lines are experimental data from the present experiments, and the distinct points are Mochizuki and Yang's experimental results,

transcribed from Figure 5 in their article [5]. Similar Reynolds numbers were examined between our work and Mochizuki and Yang's to determine the validity of our results. It can be easily seen that the initial behavior, and the behavior in the final third of the channel match very closely in both trends and magnitude. The troughs that are observed in Mochizuki and Yang's work are noticeably absent in our experimental data set.

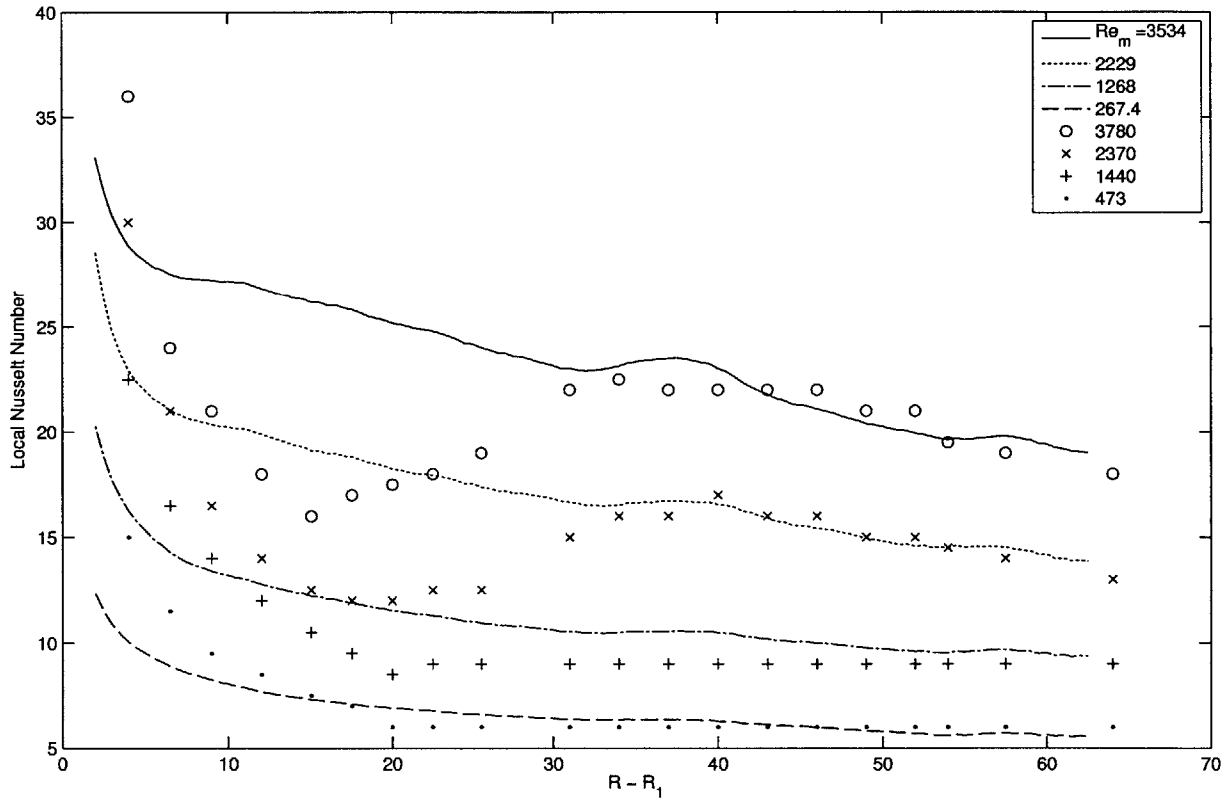

Figure 3-1: Pressure driven flow of nitrogen at various mean Reynolds numbers compared directly to Mochizuki and Yang's results. Experimental results taken with a gap of 0.8 mm, and represented as lines. Mochizuki and Yang's results represented as distinct points.

Mochizuki and Yang state that the cause of the trough is due to the transition from a pure laminar flow regime to an oscillating laminar flow regime. The oscillations cause an increased heat transfer coefficient, and therefore describe the local increase in heat transfer. This transition is completely absent in this work's experimental data set.

Mochizuki and Yang's experimental apparatus is significantly different in two respects

to ours. First, the entrance to the channel in their experiments is a rounded corner, while ours is at a right angle. Secondly, the flow channel in their experiments is relatively smooth, while ours is extremely rough because of the wire traces on the heated disks. The surface roughness defined as

$$Roughness\ Ratio = \frac{\epsilon}{b_{gap}}, \tag{3.3}$$

has a value of 0.05 in Figure 3-1's experiment [8]. This surface roughness will significantly effect turbulent flow characteristics, and will likely trip turbulence earlier in the channel than in the smooth channels of Mochizuki and Yang. The entrance effect and the roughness effect are expected to compound, causing an early onset of unstable flow characteristics, which then correspondingly increase heat transfer because of increased mixing. This explains the lack of the troughs in this particular data set. To create similar dimensionless quantities to Mochizuki and Yang's work it was necessary to impose a significantly lower gap thickness than used in all other experiments in this work. The lower gap thickness causes a more pronounced roughness and entrance effect.

In an experiment with a gap 2.5 times wider (and similar to the rest of the present experiments), the troughs described in Mochizuki's experiments begin to appear. When the gap is larger, the roughness ratio proportionally decreases, and it is also expected that the entrance region effect will be less significant. These results are shown in Figure 3-2, but are quantitatively incomparable to Mochizuki and Yang's results because of the different range of dimensionless radius. The quantitative agreement in the small gap experiments combined with the qualitative agreement in the large gap experiments shows the agreement in observed fluid mechanic phenomena and heat transfer rates between Mochizuki and Yang's results and ours. The rest of the experiments are conducted with larger gaps to accommodate the impeller, which reduces the entrance and roughness effects observed in Figure 3-1.

In both Figures 3-1 and 3-2 bumps can be seen at $R - R_1 = 40$ and $R - R_1 = 15$, respectively. These become larger at higher Reynolds numbers, and are artifacts of the experimental apparatus. During the course of testing, one of the heated region's wire increased

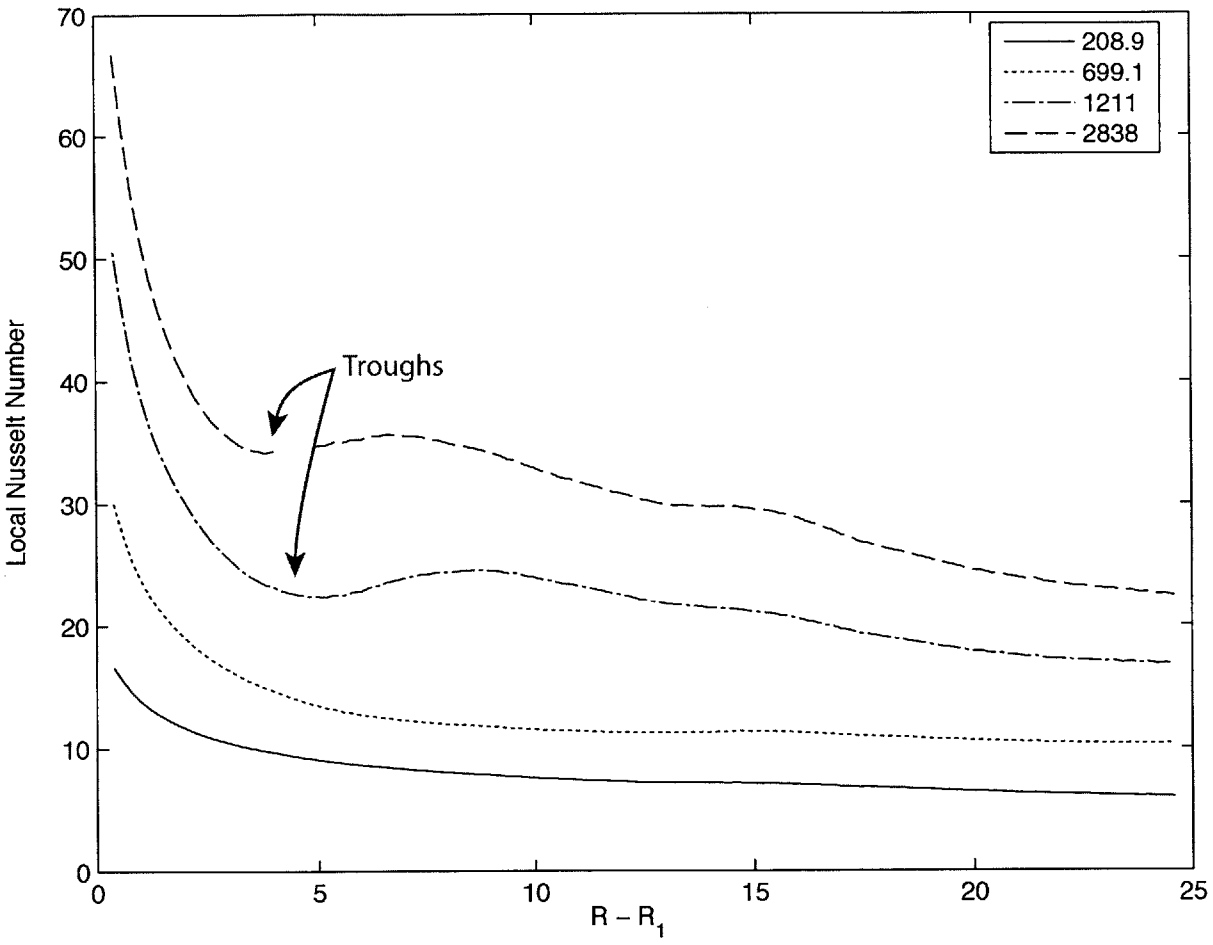

Figure 3-2: Pressure driven flow of nitrogen at various mean Reynolds numbers, with a gap thickness of 2 mm. The troughs shown in Mochizuki and Yang's results begin to appear here.

significantly in resistance. This was likely due to a problem in a connector. Because of this the heated region is cooler than it is predicted to be, and therefore results, after analysis, in an erroneously high heat transfer value. This is fixed in post-processing in the constant heat temperature tests, but can not be in the constant heat flux tests. These bumps should be ignored, as they do not represent any physical phenomena, but instead a systematic error in experimentation.

Pressure driven tests with the constant temperature boundary condition were also performed. Figure 3-3 shows the transition from the laminar to oscillating laminar flow regime.

The test with $Re_m = 373$ has a consistently low Nusselt number and decays, indicating a laminar boundary layer along the entire length of the plate. The second test depicted ($Re_m = 2200$) in Figure 3-3 shows a similar initial behavior, although with a higher Nusselt number because of higher mass flow rate, and then a significant jump in Nusselt number, and then a slow decay. This is indicative of a laminar to laminar oscillating flow transition. This flow is described in Mochizuki and Yang [5]. Once the flow steps into the laminar oscillating regime, the heat transfer is significantly enhanced because of mixing and vortices, which cause an effectively shorter thermal boundary layer. Mochizuki and Yang report a critical number Reynolds of approximately 1200 for the transition from laminar to laminar oscillating. While the present experimental apparatus does not allow in-stream measurement of Reynolds number, the mean Reynolds number as calculated using mass flow rate shown in Equation 3.1 shows that the first test stays well below the critical Reynolds number, and the second is above.

Figure 3-3 can be used to observe the difference between flow with and without a rotating impeller. If the flow with the impeller demonstrates similar characteristics to that of a higher Reynolds number then it can be postulated that the impeller is onsetting turbulent or laminar oscillating characteristics in the channel.

3.2 Heat Transfer Enhancement from Rotating Impeller

To examine the effect of a rotating impeller, tests with constant mass flow rates were compared. This allows the examination of the effect of the rotating impeller independent of the fluid that it forces through the channel. An improvement in heat transfer can then be directly contributed to either an increase in turbulent mixing or boundary layer shedding. Figure 3-4 depicts a representative test, which shows the enhancement of heat transfer over pure pressure driven flow due to an impeller at different speeds with constant Reynolds number. As is evident, when the impeller is rotating faster, the heat transfer is enhanced over the entire disc.

To examine the phenomena behind the enhancement of heat transfer, a comparison is

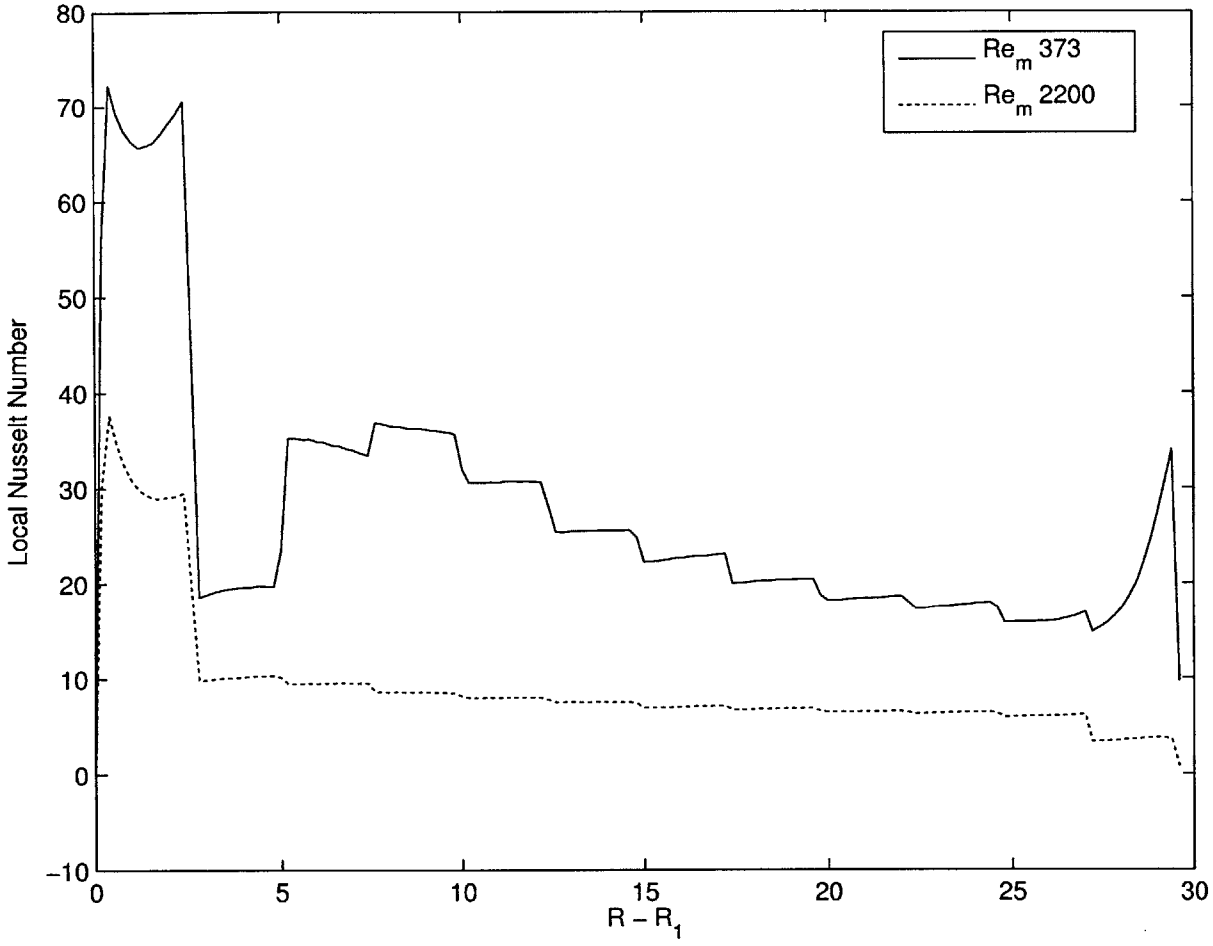

Figure 3-3: Pressure driven flow of nitrogen with constant temperature boundary condition. The difference between a constant laminar boundary layer and a transition from laminar to laminar oscillating is evident.

made between the pressure driven flow and the flow with a rotating impeller with various mass flow rates. This comparison is depicted in Figure 3-5. The pressure driven curve with no fan is the same curve as displayed in Figure 3-3 that showed the transition from laminar to laminar oscillating flow. The middle curve is a test at a lower Reynolds number, but with a fan rotating at 9000 RPM. The behavior is similar to the first curve, but with seemingly no initial laminar boundary layer impeding heat transfer.

From Figure 3-5 it is evident that the addition of the impeller changes the overall fluid mechanic properties of the channel. If the impeller simply increased the effective Reynolds

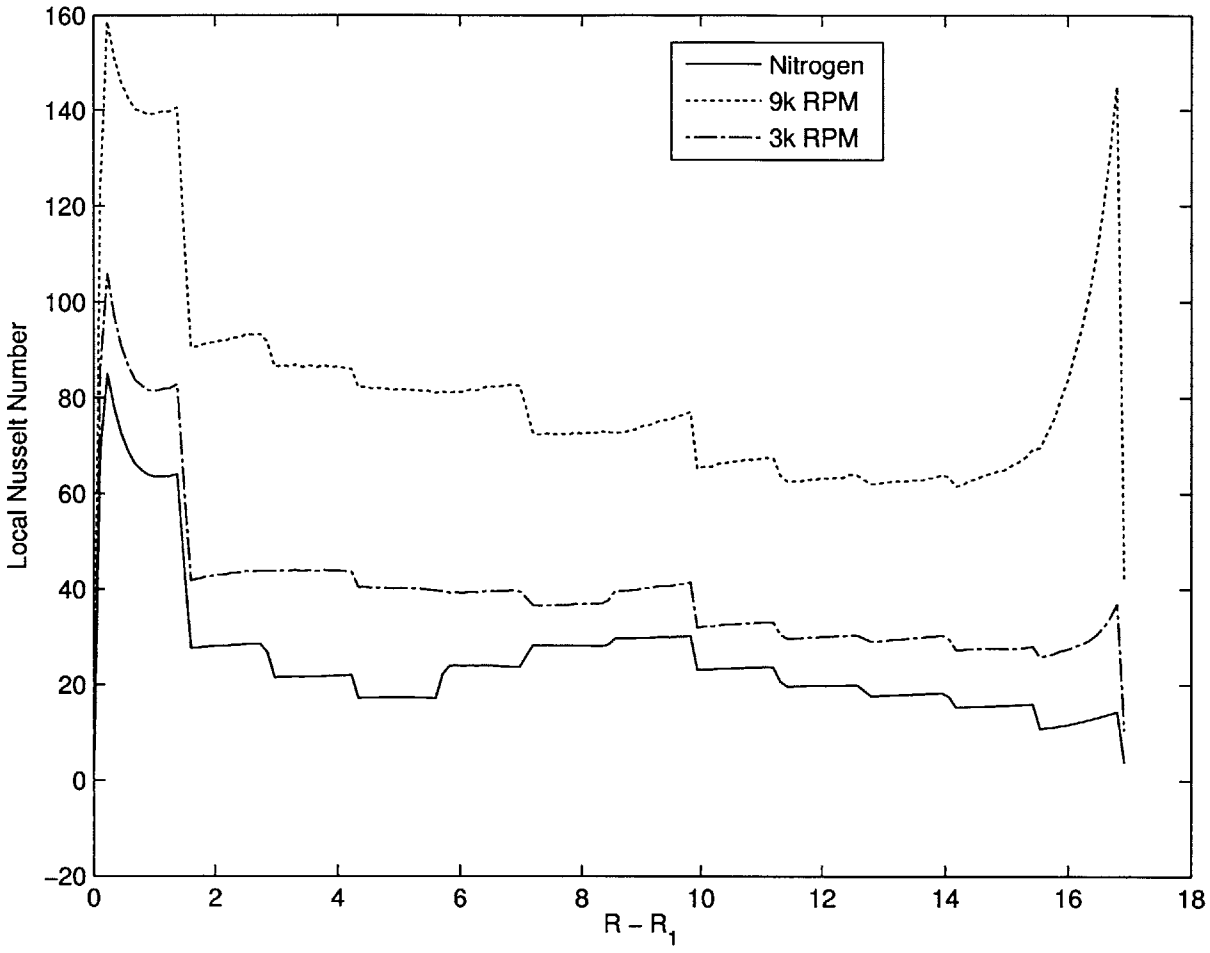

Figure 3-4: Comparison of Nusselt Numbers with an approximately constant mean Reynolds number of 1150 at different impeller speeds. The nitrogen test corresponds with a zero RPM impeller speed.

number, then a transition between laminar and laminar oscillating would be seen, as it is in the pressure driven experiments. In the pressure driven experiments, enhancement in heat transfer is caused by a transition to oscillating laminar flow, which correspondingly decreases the thickness of the boundary layer. It is thought that the impellers also decrease the thickness boundary layer to enhance heat transfer, but with slightly different mechanisms.

Tests were performed with a fan that occupied the entire radius, and one that only extended three quarters of the way into the disk. A comparison between the performance of these fans informs about the fluid mechanics in the gap. As seen in Figure 3-6 the heat

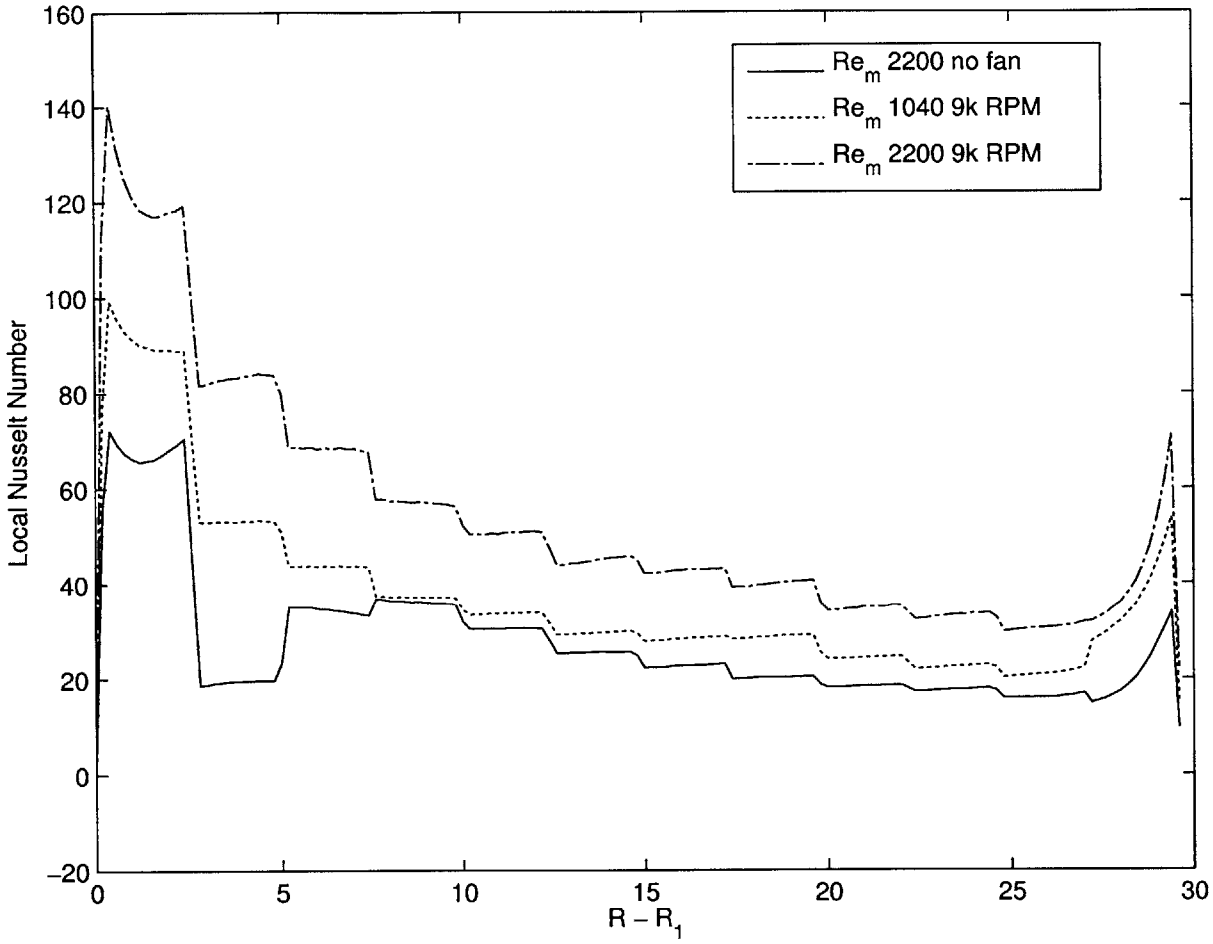

Figure 3-5: Comparison of local Nusselt Numbers with various Reynolds number with a constant gap thickness. The bottom curve has purely pressure driven flow, while the upper ones have an impeller rotating at 9000 RPM. The enhancement in heat transfer due to the impeller is evident here.

transfer characteristics are very similar between the two fans for the portion of the disk that both fans occupy. As soon as the blades end, however, in the smaller fan there is a faster decay of heat transfer than that of the larger fan. Wherever there are not spinning blades present in a channel, the boundary layer will be allowed to reform and it is expected to increase in thickness, thereby impeding heat transfer. This is observed clearly in Figure 3-6.

Three distinct regions in the channel are identified, and shown in Figure 3-7. The first is the entrance region where the boundary layer is thinner and there is very high heat transfer

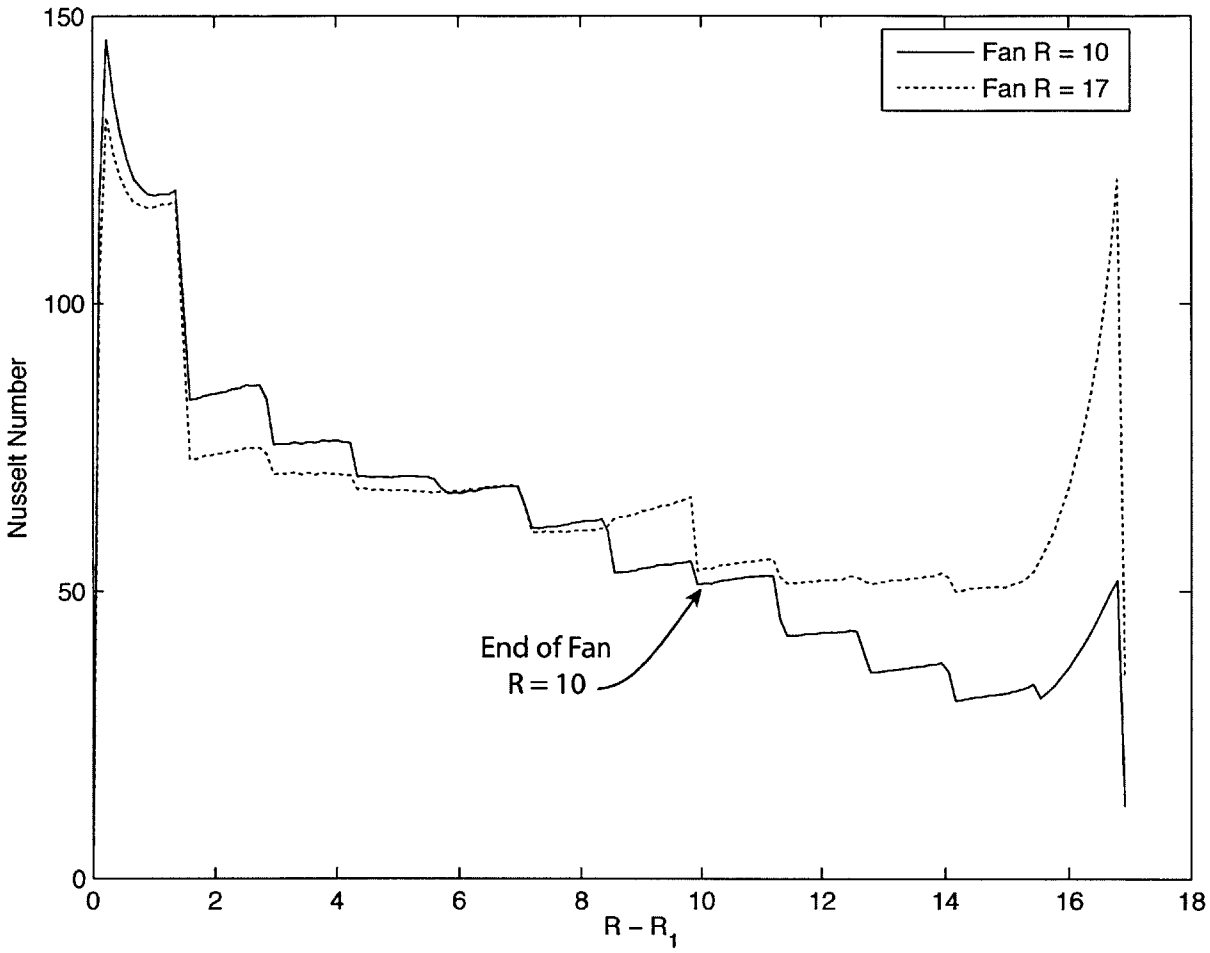

Figure 3-6: Comparison of local Nusselt Numbers with a fan that occupies the entire disk, and one that occupies only three quarters of the disk, with a constant gap and Reynolds number.

rates. The next is the central region, which occupies the bulk of the channel. The heat transfer in this region is relatively constant, and is the region of most interest because it contributes most heavily to the overall average heat transfer coefficient. The final region is the exit region, where the heat transfer coefficient is uncharacteristically high because of ingestion of ambient air for the outlet of the channel. Examining each region individually, particularly the central region, will give more insight into the fluid mechanics of the channel. The high heat transfer in the entrance and exit masks the effects that occur in the central region.

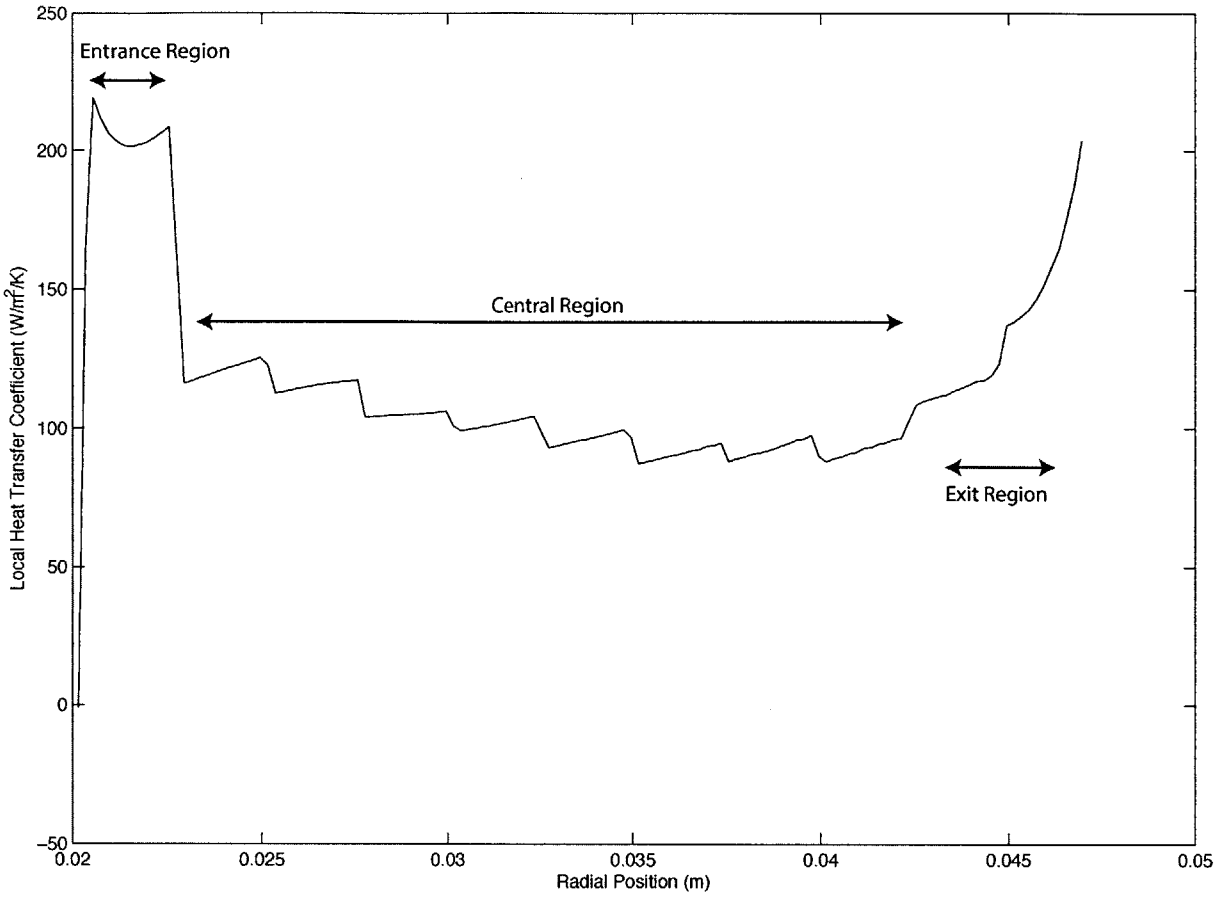

Figure 3-7: An example heat transfer test which shows the three different regions that are examined.

The relationship between mass flow rate and rotational velocity was examined further with various mass flow rates. The results of this study are shown in Figure 3-8, which is a plot of Nusselt number in the central region versus local Reynolds number. In these plots the Nusselt number scales linearly with Reynolds number and that increasing the angular velocity of the blades increases the local Nusselt number. The proportional effect of the blade velocity is unclear, because there is a change in the slope of the lines at different rotational velocity.

Tests were performed with fans with different numbers of blades to examine the mechanics of heat transfer enhancement. If the heat transfer enhancement is due to an increase in turbulent mixing, the number of blades would have a less profound effect than that of the

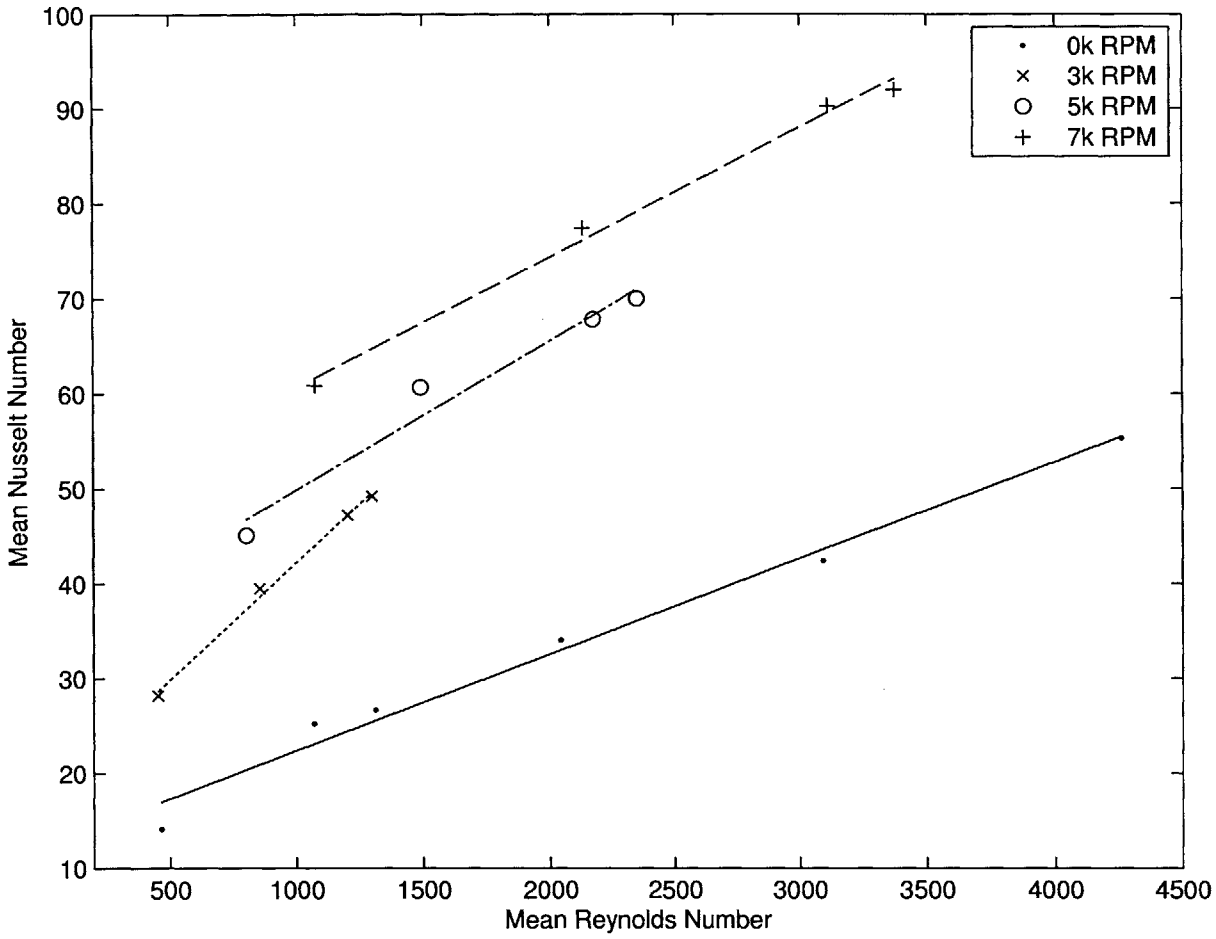

Figure 3-8: Comparison of local Nusselt Numbers with various radial Reynolds numbers and rotational velocities in the central region.

rotational speed. This is because the fan would increase the velocity of the fluid inside, thus onsetting turbulent flow. Although more blades would be able to push more fluid uniformly, this effect would not be overwhelming. On the other hand, if the enhancement in heat transfer was due to blades wiping the boundary layer, it would be expected that an increase in blade count would have a nearly identical effect as a proportional increase in rotational velocity.

Figure 3-9 shows the central region as well, but with fans with different blade counts. As in Figure 3-8 the Nusselt number scales linearly with Reynolds number, and is shifted upward by a change in speed. It is striking in this diagram that the 15 blade fan at 5000

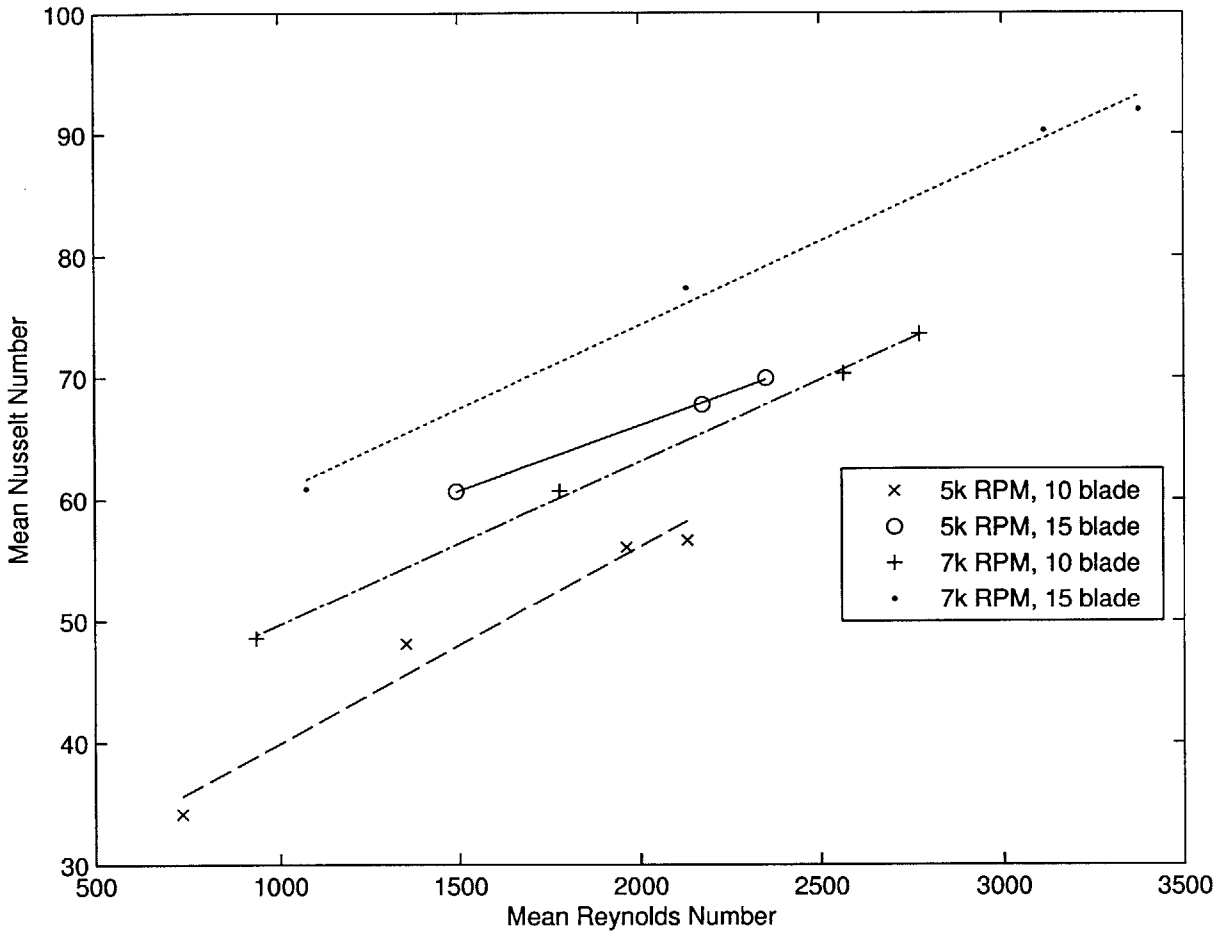

Figure 3-9: Comparison of local Nusselt Numbers with various radial Reynolds numbers and rotational velocities in the central region for two fans, one with 10 blades and one with 15 blades.

RPM has higher heat transfer than the 10 blade fan at 7000 RPM. The ratio in blade count is 1.5 ($\frac{15\,blades}{10\,blades}$), and the ratio in speeds is 1.4 ($\frac{7000\,RPM}{5000\,RPM}$). So, if the blade count is just as important as the rotational speed of the impeller, as is predicted by the boundary layer shedding, then the 15 blade fan test at 5000 RPM should perform slightly better than the 10 blade fan test at 7000 RPM. This is exactly what occurs, supporting the boundary layer shedding theory.

The renewal frequency is the number of times a blade passes over a given section per second. This is given by:

$$f = rotational\,velocity \times blade\,count \tag{3.4}$$

If the surface renewal theory is accurate then renewal frequency should contribute to heat transfer directly, without the need to know rotational speed or blade count explicitly. Theory predicts that heat transfer scales with the square root of renewal frequency, as shown below [2].

$$h = 2\sqrt{\frac{k\rho c_p}{\pi}}\sqrt{f} \tag{3.5}$$

It is then postulated that Nusselt number is proportional to frequency based Reynolds number times radial Reynolds number.

$$Nu \propto (Re_{radial} \times Re_f)^{\alpha} \tag{3.6}$$

Figure 3-10 shows the Nusselt number for the central region as a function of $Re_f \times Re_{radial}$, for blades speeds between 3000 and 7000 RPM. It can be seen that the data very closely follows a power function as postulated. This fit is:

$$Nu = 6.7 \times 10^{-3}(Re_{radial} \times f)^{0.46} \tag{3.7}$$

and yields an R-square value of 0.95. The closeness of this fit is a compelling argument for the validity of the surface renewal theory. In Staats' work surface renewal theory was discarded because the average heat transfer coefficient did not agree with the theoretical predictions. Because the entrance and exit effects in these experiments is very high, and often unpredictable, as can be seen in Figure 3-4, the average heat transfer in the channel can be significantly different from the properties in the middle of the channel. Because of this, it is expected that an examination of the local properties in the middle of the channel could be different from the overall total properties.

All three regions in the channel are next investigated. Figure 3-11 shows the same tests as are shown in Figure 3-10, with a logarithmic scale, and in the three separate regions of

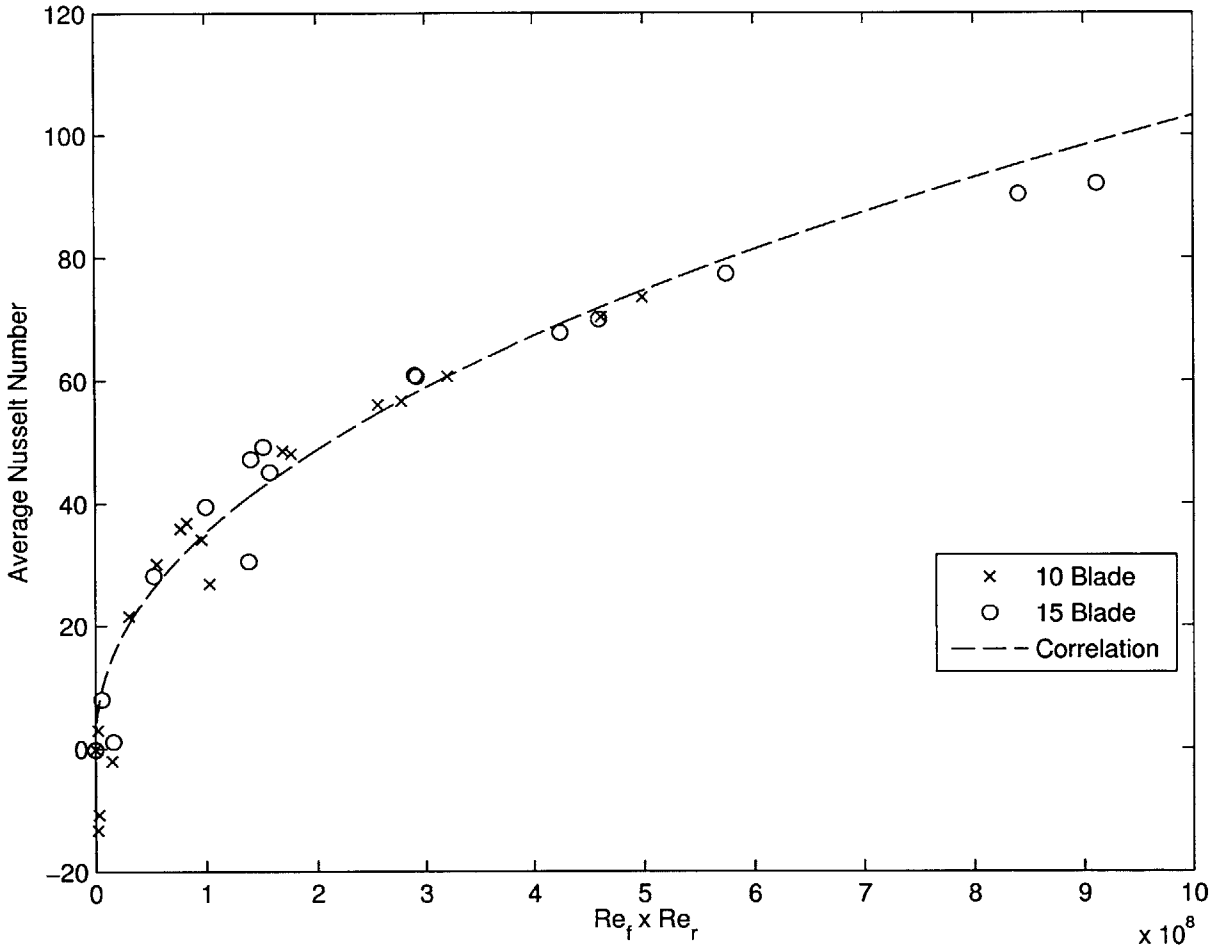

Figure 3-10: Comparison of Nusselt Numbers as a function of $Re_f \times Re_{radial}$, in the central region for two fans, one with 10 blades and one with 15 blades. A power fit is shown, with an R-square value of 0.95. Tests conducted at a gap thickness of 3.5 mm.

the channel. In the innermost portion of the channel the entrance effect is significant, and results in a significant enhancement in heat transfer over the rest of the channel. In the center of the channel it can be seen that the correlation accurately predicts both the ten and fifteen blade fans. At the exit of the channel the correlation accurately matches the heat transfer performance in the high $Re_f \times Re_r$ region, while in the lower region it is higher than the correlation predicts. This is due to the high recirculation that occurs at the exit of the channel. In the higher flow regimes this effect is negligible compared to the surface renewal and mass flow rate radially outward.

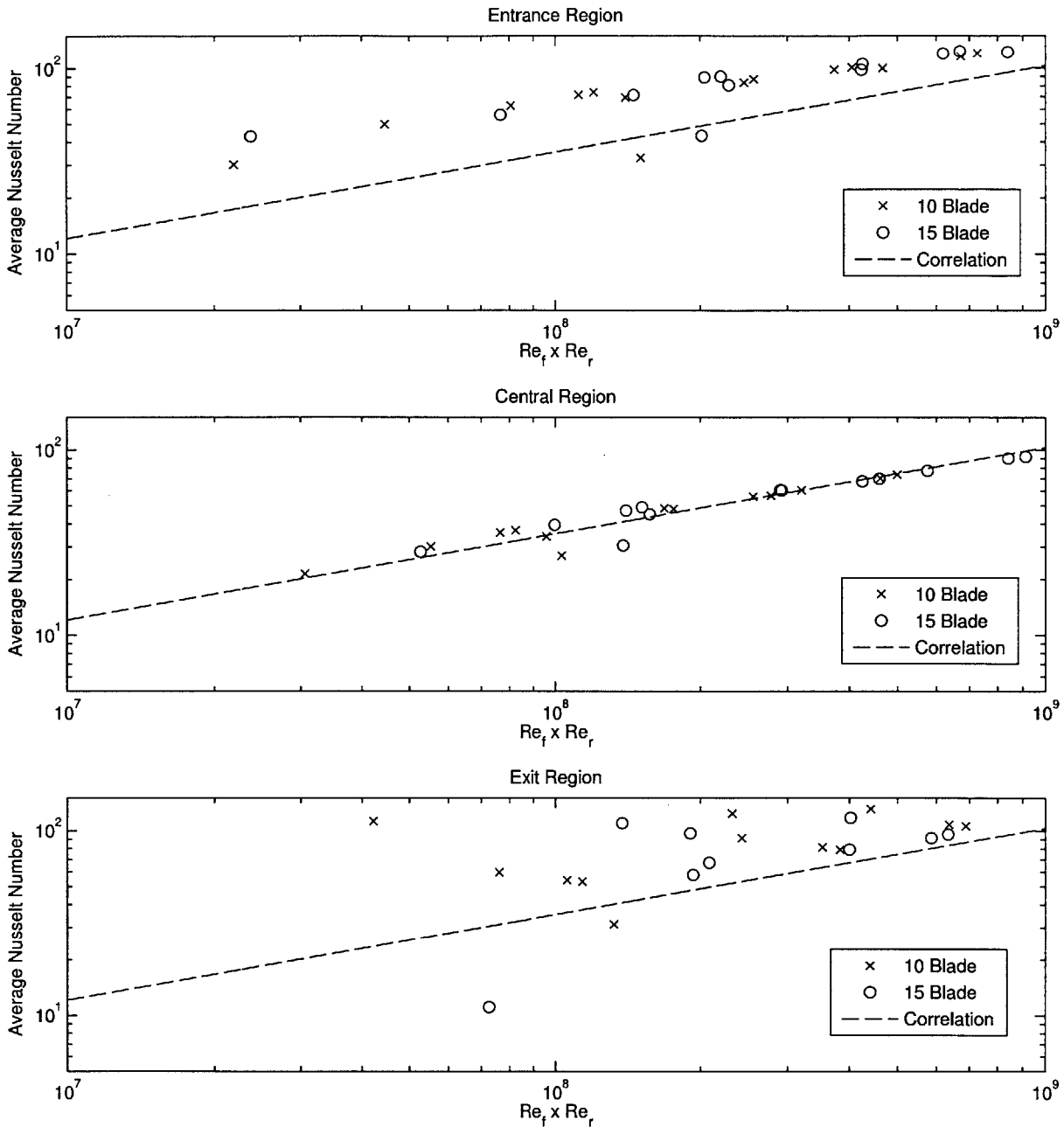

Figure 3-11: Comparison of local Nusselt Numbers as a function of $Re_f \times Re_{radial}$, in three different regions of the channel. Tests were conducted with a fan with 10 blades, and one with 15 blades. All three correlations are the same, and demonstrate the relative difference in heat transfer between different regions in the channel.

The difference in heat transfer between different regions, as shown in Figure 3-11, causes the masking of fluid mechanic behavior in the average heat transfer coefficient. The average heat transfer coefficient bundles the bulk properties of the channel, the entrance effect, and the recirculation effect, clouding the properties in the center of the channel. This causes the discrepancy found in this work and the work on average heat transfer coefficient done by Staats.

Experiments varying gap thickness were performed to determine the effect of gap on heat transfer. As before, the center of the channel is specifically examined to eliminate the recirculation and entrance effects. Figure 3-12 shows tests with the same fan (a $75\,mm$ OD, 15 blade) with varying gap thickness. In this comparison, the Nusselt number is calculated with the flow length ($Nu = hL/k$, $L = r_2 - r_1$) instead of the hydraulic diameter to compare the difference in heat transfer without scaling the Nusselt number with gap thickness. This allows an absolute comparison between the tests.

Figure 3-12 shows the slight enhancement of heat transfer with smaller gap thicknesses. This is consistent with boundary layer shedding, because as the fan blade moves closer to the surface, it will shear more of the boundary layer away. The results are clearer as $f \times Re$ increases because the effect of the rotating impeller dominates the recirculation effect in this area. The enhancement of heat transfer in smaller gap scenarios is encouraging from a design perspective because it yields a more volumetrically efficient device.

A constant mass flow rate using a closed loop controller was imposed across various rotational velocities. This allows the examination of the effect of the frequency renewal independent of the radial Reynolds number.

Figure 3-13 shows average Nusselt number in the central region versus rotational velocity for two separate, constant, mass flow rates. The Nusselt number scales linearly with increasing rotational velocity, and the fitted slopes across the two mass flow rates vary by only 3.8%. This is strong evidence that the physical phenomena governing the results in Hagge are significantly different from those in the present work, because the results from Hagge's work found that heat transfer varied with the square root of rotational velocity.

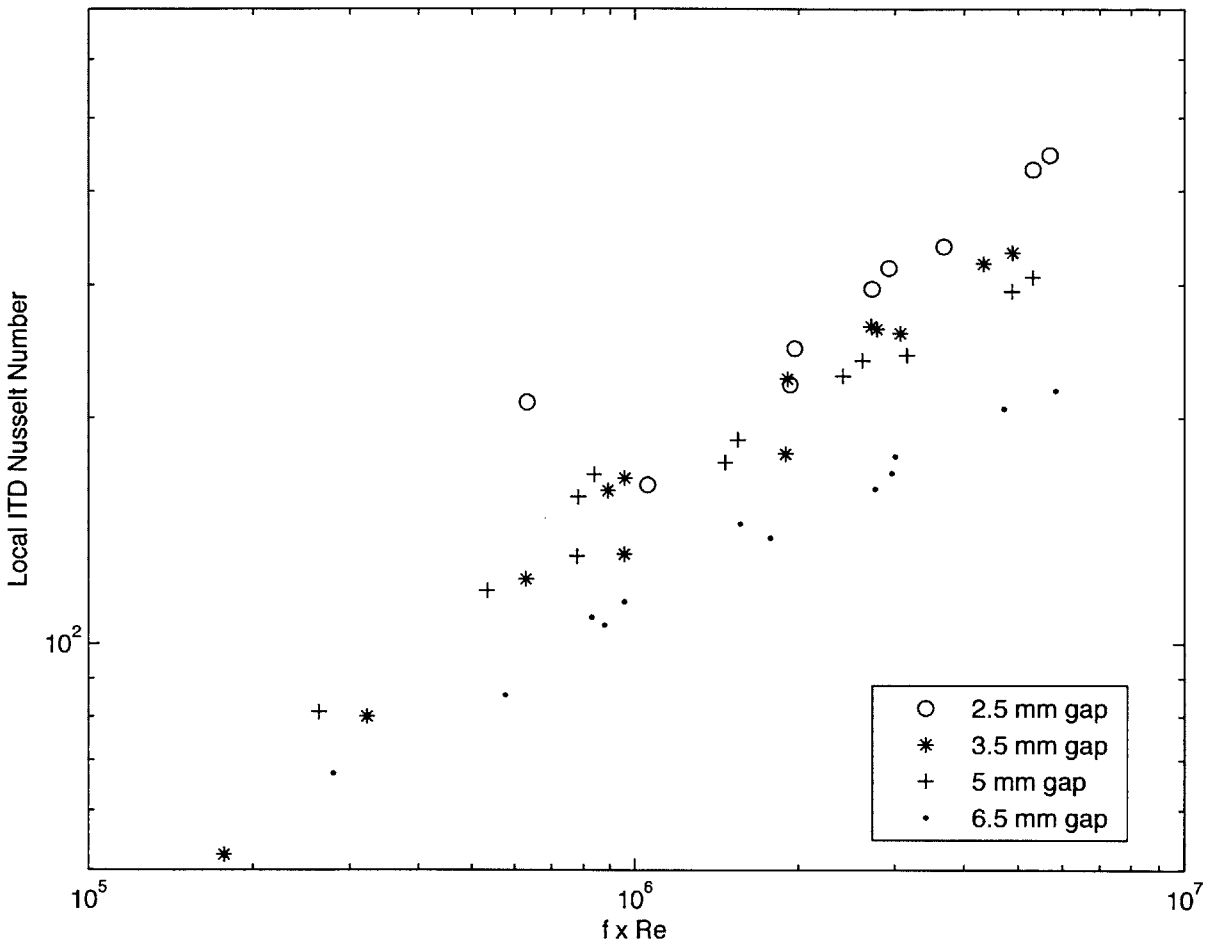

Figure 3-12: Comparison of local Internal Temperature Difference Nusselt Numbers as a function of $f \times Re_{radial}$, with four different gap thicknesses. Tests were conducted with a 15 blade fan, with an outer diameter of 75 mm. It can be seen that a smaller gap slightly enhances heat transfer

Constant mass flow rate was also imposed for a ten blade impeller. Figure 3-14 shows these results for one mass flow rate. There is little variation between the heat transfer of the 15 blade impeller and that of the 10 blade impeller at various rotational velocities, and they show the same linear slope. This is strong evidence against the hypothesis of surface renewal frequency, because if the surface renewal hypothesis is valid, a clear enhancement would be seen in the heat transfer of the 15 blade fan over that of the 10 blade fan.

The previous results that indicated that surface renewal frequency was a determining

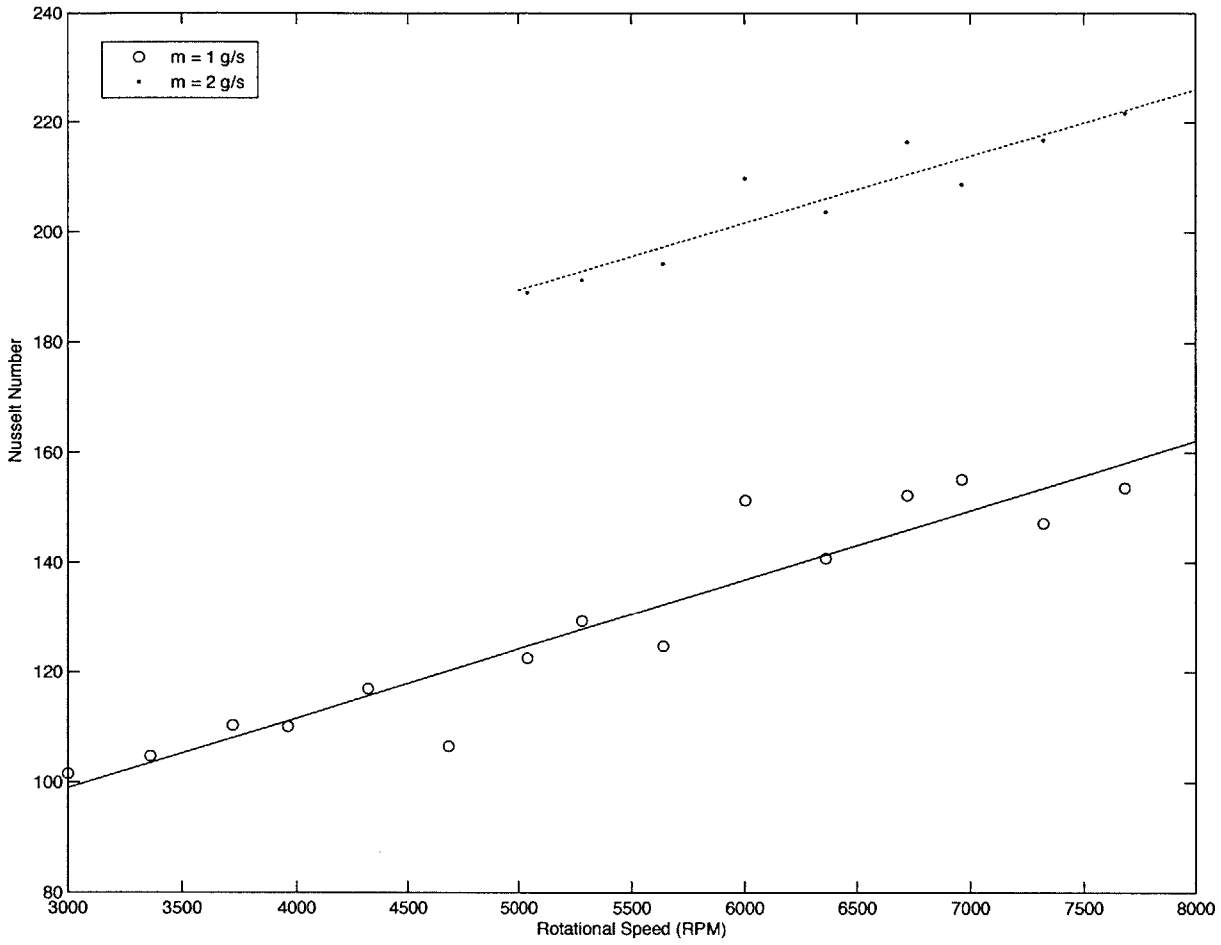

Figure 3-13: Nusselt number with various impeller speeds, all at a constant mass flow rate, averaged over the central region of the channel. Tests taken at a gap thickness of 3.5 mm and with the 15 blade impeller.

factor in performance must be due to the differing pumping properties of the fans. Because previous results used a coupled $f \times Re$, they mask the individual contribution of frequency renewal and differing mass flow rate. Future experimentation varying the mass flow rate through a wide range of values while keeping impeller speed constant would be useful for determining the nature of the fluid flow.

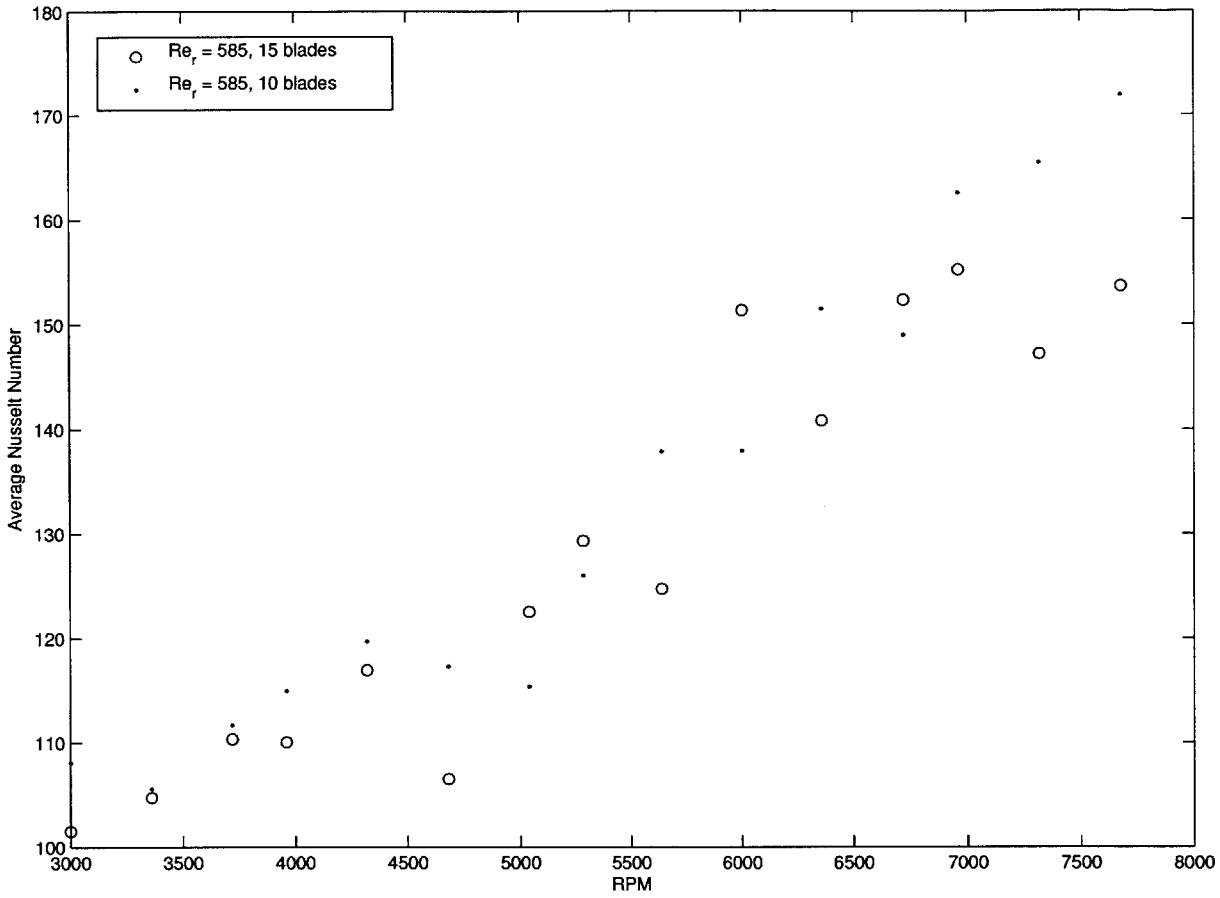

Figure 3-14: Nusselt number with various impeller speeds, all at a constant mass flow rate, averaged over the central region of the channel. Tests taken at a gap thickness of 3.5 mm and with both the 15 and 10 blade impellers.

3.3 Future Work

It is desired to further decouple the relationship between rotational velocity of the impeller and mass flow rate (radial Reynolds number). This will be done by imposing a constant rotational velocity in the impeller and varying the mass flow rate by changing the throttle position. It is hypothesized that the heat transfer can be approximated by some correlation that follows:

$$Nu = \alpha Re_\omega + f(Re_r) \tag{3.8}$$

Future work will try to determine the radial Reynolds number component of Nusselt number.

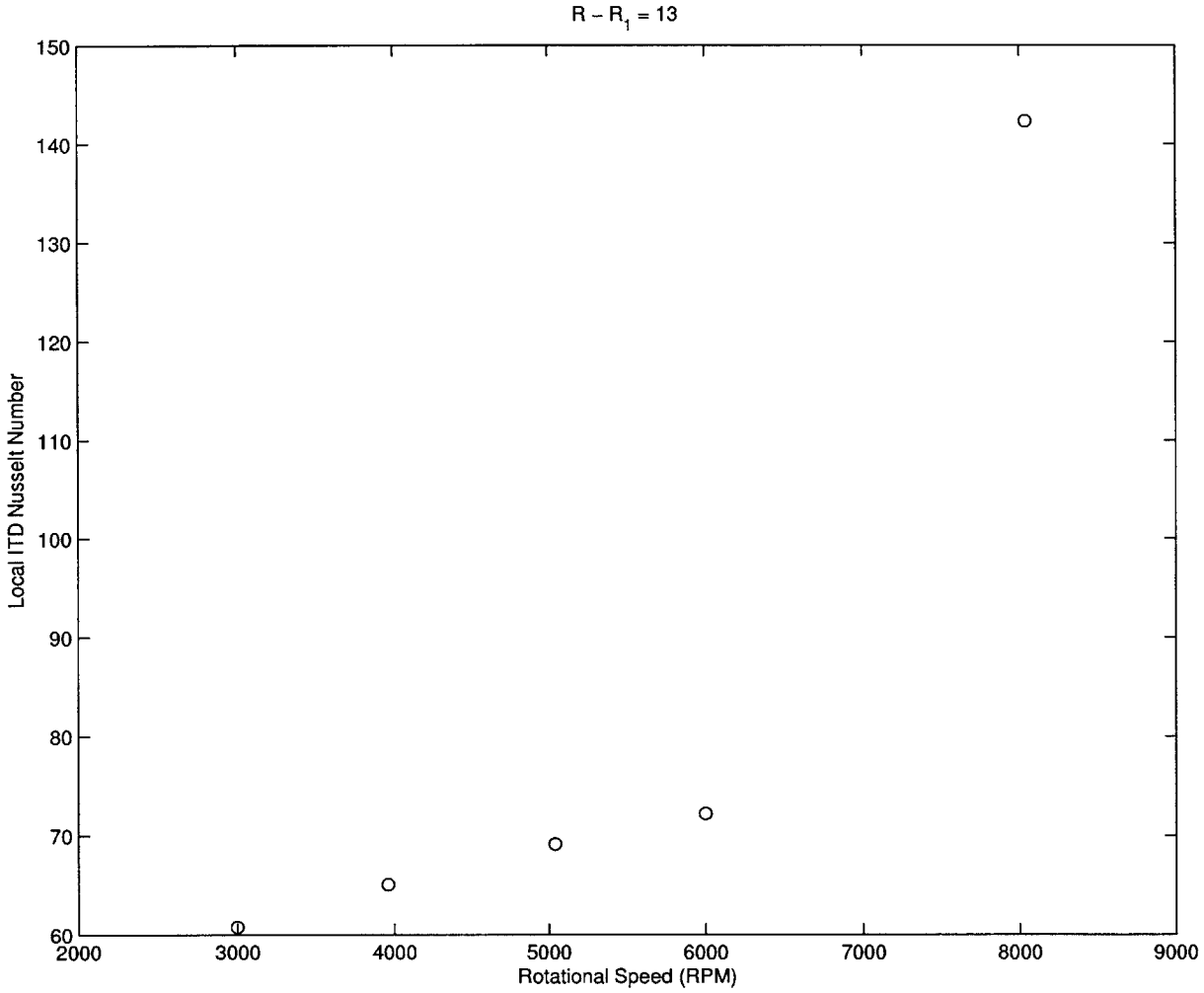

Figure 3-15: Comparison of local Nusselt Numbers as a function of rotational velocity with mass flow kept constant under a PI-control system. The large increase in heat transfer at 8000 RPM is indicative of a flow transition.

It is thought that there is a flow transition occurring at approximately 8000 RPM. This can be seen throughout the experimental results, and is particularly evident in Figure 3-4. Initial results from the controlled mass flow system show the flow transition occurring at 8000 RPM, as shown in Figure 3-15. The experimental apparatus does not have a motor capable of comfortably examining the transition, and large uncertainty begins to appear at high motor speeds ($\sigma_{motor} = 60$). It would be beneficial to examine this flow transition

in later work, because operating in this region has potential to significantly enhance heat transfer in the heat sinks.

Chapter 4

Conclusions

The experimental apparatus used in this work was used to obtain measurements of heat transfer of pressure induced radial flow between parallel plates. The results of the measurements agreed with previous work done on these flows. Following this impellers were installed into the apparatus and were spun at several speeds as additional heat transfer measurements were made. The impeller was seen to provide up to a five-fold improvement in heat transfer over the entire length of the channel with a constant mass flow rate. It was also shown that the presence of the impeller blades in the channel directly improves heat transfer, as was seen in the comparison of large and small impellers. The enhancement in heat transfer can be then attributed to fluid agitation caused by the impeller blades. The improvement in heat transfer was initially thought to be proportional to surface renewal frequency, or the number of times a blade passes over a specific region, not the blade count or rotational velocity explicitly. The behavior of the heat transfer coefficient between the air and the plates changes as the air flows radially outward between the plates. In the first region, characterized by entrance effects, the heat transfer coefficient is high. This is followed by a second, or central region, where the heat transfer coefficient does not vary significantly. Finally, there is a third region of uncharacteristically high heat transfer coefficients due to the fluid ingestion from the exit of the flow from the two plates. In this work, a correlation was found that predicts the heat transfer in the central region, and is proportional to the product of radial Reynolds

number and surface renewal frequency. It was determined that, in the central region, the heat transfer coefficient is weakly dependent on the distance between the heated plates, with higher heat transfer found with a narrower gap spacing. Using tests of constant mass flow rate, it was determined that the heat transfer rate is not determined by the surface renewal frequency, but simply the rotational velocity of the fan, which shows that the heat transfer enhancement from the impellers is due to an increase of turbulent mixing within the channel.

It is suspected that there is a flow transition occurring at high rotational velocities (8000 RPM or higher) which merits further investigation, but was not possible with the current experimental apparatus. It is also desired to further decouple the effect of radial Reynolds number and surface renewal frequency. This will be investigated in later work.

Bibliography

[1] T. Bergman F.P. Incropera, D.P. DeWitt. *Fundamentals of Heat and Mass Transfer.* John Wiley and Sons, 2006.

[2] G.H. Junkhan J.K. Hagge. Mechanical augmentation of convective heat transfer in air. *Journal of Heat Transfer*, 97(4):516–520, 1975.

[3] M. McCarthy D. Jenicek A.K. Edoh J. H. Lang E. N. Wang J.G. Brisson J.M. Allison, W.L. Staats. Enhancement of convective heat transfer in an air-cooled heat exchanger using interdigitated impeller blades. *International Journal of Heat and Mass Transfer*, 54:4549–4559, 2011.

[4] Wen-Jei Yang S. Mochizuki. Self-sustained radial oscillating flows between parallel disks. *Journal of Fluid Mechanics*, 154:377–397, 1985.

[5] Wen-Jei Yang S. Mochizuki. Local heat-transfer performance and mechanisms in radial flow between parallel disks. *Journal of Thermophysics*, 1(2):112–116, 1987.

[6] W. Staats. *Active Heat Transfer Enhancement in Integrated Fan Heat Sinks.* PhD thesis, Massachusetts Institute of Technology, August 2012.

[7] Molly Webb. Smart 2020: Enabling the low carbon economy in the information age. Technical report, The Climate Group, London, UK, 2008.

[8] F.M. White. *Fluid Mechanics.* McGraw-Hill, 2003.